Enhanced Evaluation of hourly and Daily Extreme Precipitation in Norway from Convection-Permitting Models at Regional and Local Scales

Kun Xie[1,2], Lu Li[3], Hua Chen[1,2], Stephanie Mayer[3], Andreas Dobler[4], Chong-Yu Xu[5], Ozan Mert Gokturk[3]

[1]State Key Laboratory of Water Resources and Hydropower Engineering Science, Wuhan University, Wuhan

430072, P. R. China

[2]Hubei Provincial Key Lab of Water System Science for Sponge City Construction, Wuhan University, Wuhan,

China

[3]NORCE Norwegian Research Centre, Bjerknes Centre for Climate Research, Bergen, Norway

[4]The Norwegian Meteorological Institute, Oslo, Norway

[5]Department of Geosciences, University of Oslo, P.O Box 1047 Blindern, 0316 Oslo, Norway

Correspondence to: Hua Chen (chua@whu.edu.cn); Lu Li (luli@norceresearch.no)

Abstract

Convection-permitting regional climate models (CPRCMs) have demonstrated enhanced capability in capturing extreme precipitation compared to regional climate models (RCMs) with convection-parameterization schemes. Despite this, a comprehensive understanding of their added values in daily or sub-daily extremes, especially at local scale, remains limited. In this study, we conduct a thorough comparison of daily and sub-daily extreme precipitation from the HARMONIE-Climate (HCLIM) model at 3 km resolution (HCLIM3) and 12 km resolution (HCLIM12) across Norway's diverse landscape, divided into five regions, using both gridded and in-situ observations. Our main focus is to investigate the added value of CPRCMs (i.e., HCLIM3) compared to RCMs (i.e., HCLIM12) for extreme precipitation at daily and sub-daily scales from regional to local scales, and quantify to what extend CPRCMs can reproduce the orographic effect on extreme precipitation at daily and sub-daily scale. We find that HCLIM3 better matches observations than HCLIM12 for daily and hourly extreme precipitation across all grid points in Norway, while HCLIM12 underestimates the extremes, especially for hourly extremes. At the regional scale, HCLIM3 captures the maximum 1-day precipitation (Rx1d) and maximum 1-hour precipitation (Rx1h) more accurately across most regions and seasons, except summer. Besides, HCLIM12 underestimates daily return levels across most regions while HCLIM3 shows larger bias of daily extreme in the east and west at the local scale. Nevertheless, HCLIM3 consistently demonstrates added value in simulating daily extremes in the middle and north regions at both regional and local scales, as well as hourly extremes at all 10 stations, compared with HCLIM12. Both HCLIM3 and

HCLIM12 capture the seasonality of extreme precipitation well across most regions, with HCLIM3 outperforming HCLIM12 for hourly extremes. Additionally, the reverse orography effect on seasonal Rx1h and Rx1d is well captured, with HCLIM3 showing added value in representing the reverse orographic effect of daily extremes except in summer. This study highlights the importance of more realistic convection-permitting regional climate simulations in providing reliable insights into the characteristics of precipitation extremes across Norway's five regions. Such information is crucial for effective adaptation management to mitigate severe hydro-meteorological hazards, especially for the local extremes.

1 Introduction

In recent years, the world has witnessed a surge in both frequency and intensity of floods primarily attributed to the increasing occurrence of intensive rainfall events (Tabari, 2020). These changes underscore the pressing need to develop a predictive understanding of precipitation extremes for the upcoming decades, given the ongoing globe warming. The intensification of precipitation extremes under the influence of global warming has the potential to trigger severe natural hazards and exert significant socioeconomic impacts (Thackeray et al., 2022), which has gained substantial attention in recent research endeavors. However, most previous research in this field relied on coarse-resolution GCMs with grid sizes exceeding 100 km, which struggle to accurately simulate extreme precipitation events and their frequency due to the limitations of their coarser resolution (Piani et al., 2010; Wang et al., 2017). Notably, these GCMs tend to produce the largest errors in predicting extreme precipitation, particularly in cases involving heavier convective activity, as observed in the study by Gervais et al. (2014a). Despite various bias-correction techniques are applied to mitigate these discrepancies on the GCMs, as well as employing them as forcing data for regional climate models (RCMs) with grid size larger than 10 km, it remains a persistent challenge to eliminate the transfer of biases from GCMs to RCMs, as noted by studies such as Pontoppidan et al. (2018) and Kim et al. (2020). The large resolution gap between GCMs or RCMs and localized precipitation extremes further constrains the robust simulations of extreme precipitation as highlighted by Li et al. (2020a). In addition, the reliance on parameterization schemes to represent convection in these coarse resolution models introduces a significant source of uncertainty in modelling errors (Prein et al., 2015; Kendon et al., 2019). More frequent and intense precipitation events under global warming stimulate interest in higher resolution and physics-based models to improve the estimation of short-duration extremes.

Convection-permitting regional climate models (CPRCMs), with grid size of less than 4 km, offer a promising alternative, which explicitly represent convection, eliminating the need for parameterizations of deep atmospheric convection. The potential in resolving deep convection and local extremes from CPRCMs lead to the realistic representation in daily and sub-daily precipitation features, including diurnal cycle, intensity and frequency of heavy precipitation events, seasonality, spatial-temporal pattern, wet-spell and dry-spell. For instance, CPRCMs have been proven to reduce the bias and enhance the representation in precipitation intensity and intensity in the Tibetan Plateau, the highest highland in the world, as shown in Li et al. (2021). In addition to their capability in capturing precipitation, Liu et al. (2017) also demonstrated the confidence of CPRCMs in estimating snowfall and snowpack

68 in the central U.S. Furthermore, the importance of CPRCMs in representing dry spell, dry and wet extremes induced

69 by local convective activity across Africa has also been found in Kendon et al. (2019), Chapman et al. (2023) further

70 confirmed its benefit in capturing rare rainfall extreme and local feature. In UK, Kendon et al. (2023) and Kent et al.

71 (2022) have found the benefit of CPRCMs compared to RCMs with convection parameterization schemes.

72 Additionally, the superior performance in capturing hourly and daily extreme precipitation including return-level,

73 frequency and intensity from CPRCMs over Alpine in Europe, has also been highlighted by Adinolfi et al. (2021),

74 Dallan et al. (2023) and Giordani et al. (2023).

75 Northern Europe has been reported to experience the most increase in precipitation, as indicated by Dyrrdal et

76 al., (2023), where a novel CPRCMs have been developed within the Nordic Convection Permitting Climate

77 Projections project (NorCP) based on the convection-permitting HARMONIE-Climate model (HCLIM), cycle 38

78 (HCLIM38) at a resolution of 3 km (HCLIM38-AROME) and 12km (HCLIM38-ALADIN). For convenience,

79 HCLIM3 and HCLIM12 are used in the following to represent the regional climate models HCLIM38-AROME and

80 HCLIM38-ALADIN, respectively. HCLIMs also indicate both HCLIM3 and HCLIM12. Through comparisons of

81 seasonal precipitation, daily mean precipitation, higher-intensity daily precipitation, the diurnal of hourly

82 precipitation including frequency and intensity from HCLIM3 and HCLIM12 over Fenno-Scandinavia, Lind et al.

83 (2020) emphasized the add-value of CPRCMs in reproducing extreme precipitation, primarily over complex terrain,

84 compared to a coarser-scale model. Médus et al. (2022) also noted that the summer diurnal cycle of frequency and

85 intensity of hourly precipitation was correctly captured in HCLIM3 compared to HCLIM12 in the Nordic region,

86 with HCLIM12 underestimating the diurnal cycle. However, the evaluation and conclusions from Lind et al. (2020)

87 and Médus et al. (2022) mainly focused on the large regional and country scale of Fenno-Scandinavia, overlooking

88 the added values of CPRCMs at local scale. Furthermore, Thomassen et al. (2023) observed that HCLIM3 tends to

89 exhibit underestimations in monthly precipitation and a later evening peak compared to sub-kilometre models. They

90 found that the advantages of sub-kilometer models were not outstanding. These evaluations were based on gridded

91 datasets, which introduce uncertainty at the local scale, especially over complex orography (Lussana et al., 2019).

92 As Chapman et al. (2023) demonstrated, who underscored the importance of assessing rare extreme rainfall events

93 in eastern African using convection-permitting models and parameterization convection models at both grid and

94 station scales, that the extreme from grids representing rainfall averaged over a larger area are damped and hence the

95 return-level will be smaller than observation. They found that the station-derived shape parameters and return levels

96 are aligned with observations and suggested the significance of site-specific analysis and evaluations. The error

97 induced by station density in gridded dataset has also been indicated in Gervais et al. (2014b), who suggested the

98 source of large errors in gridded dataset when station density is low. Consequently, a comprehensive evaluation and

99 analysis of the added value from CPRCMs compared with RCMs that incorporates both regional and local scales is

100 crucial for extreme precipitations.

101 We acknowledge that Norway, a Nordic country, is representative of diverse climate features due to its

102 extended latitude, rugged coastline, plateaus, and complex orography. The dominances of precipitation between the

103 coastal and inland regions over Norway are distinctly different, and most of studies focusing on the hydrology and

104 meteorology over Norway were based on the divided regions (Vormoor et al., 2016; Poujol et al., 2021; Konstali
105 and Sorteberg, 2022). By dividing region with its characteristics, a more thorough comprehension of add-value of
106 CPRCMs in capturing extreme precipitation can be reached. Therefore, reliable evaluation about analyzing the add-
107 value of CPRCMs in capturing extreme precipitation should be scaled to region or local scale.

108   In the complex mountain areas, extreme precipitation is triggered by the interaction of large-scale atmospheric
109 activity and local orography property, which may cause severe hydrometeorological hazards, such as flash flooding.
110 However, understanding the orographic impact in precipitation in complex orography is challenging due to sparse
111 observations (Rossi et al., 2020). The poor representation of RCMs in capturing local precipitation have been
112 indicated in Knist et al. (2020). Importantly, CPRCMs shows advantage in reproducing precipitation bias over
113 higher complex orography in the Alpine, as shown in Lind et al. (2016) and Reder at al. (2020). Furthermore, the
114 better representation of sub-daily and daily heavy precipitation from CPRCMs over the Alpine have also been found
115 in Ban et al. (2020) and Dallan et al. (2023). Marra et al. (2021) and Dallan et al. (2023) also confirmed the
116 efficiency of CPRCMs in reproducing the reverse orography effect on hourly extreme precipitation. The relationship
117 between extreme precipitation and elevation may vary depending on latitude and climate zones (Amponsah et al.,
118 2022). Rossi et al. (2020) and Mahoney et al. (2015) found the weak depend of subdaily precipitation on elevation in
119 the Colorado, USA. Opposing the orographic enhance on daily precipitation, Dallan et al. (2023) indicated the no
120 evident relation of daily precipitation on elevation. It is worth noting that the potential added value of CPRCMs in
121 representing orographic effects compared to RCMs has not been explored. Moreover, the performance of CPRCMs
122 varies with seasons, which underscores the need to explore the orographic effects on seasonal extremes. Thus, we
123 fill this knowledge gap by characterizing orographic impact on hourly and daily extreme precipitation seasonally.

124   As highlighted by Konstali and Sorteberg (2022), there can be significant uncertainties associated with the
125 interpolation of grided precipitation data. Besides, the benefit for precipitation spatial evaluation based on in-situ
126 observation has also been reported in Thomassen et al. (2023). Therefore, the evaluation of extreme precipitation
127 from HCLIM3 and HCLIM12 here, is based on both gridded precipitation and in-situ observation. Our study aims to
128 address the value of CPRCMs (HCLIM3) in capturing the characteristics of extreme precipitation in Norway,
129 comparing it with a coarser resolution model (HCLIM12) as well as both of the in-situ and gridded precipitation
130 observations. Here, our contribution to the existing literature, e.g., Médus et al. (2022), revolves around the added
131 value of CPRCMs in the extreme precipitation characteristics, encompassing a range of metrics.

132   The main objectives of this study are to: (1) enhance the understanding of convection-permitting climate
133 models and highlighting the added value of CPRCMs by comparing their effectiveness in simulating extreme
134 precipitation with that of regional climate models from regional to local scales; (2) assess HCLIM3's capability in
135 depicting orographic effects on seasonal extreme precipitation. This research explores whether the benefits provided
136 by CPRCMs are consistent in different regions driven by varying physical processes for precipitation. Finally, our
137 study delves into the analysis of the intensity and frequency of extreme precipitation events, offering insights into
138 local and regional variations.

 2 Study area and data

 2.1 Study area

141
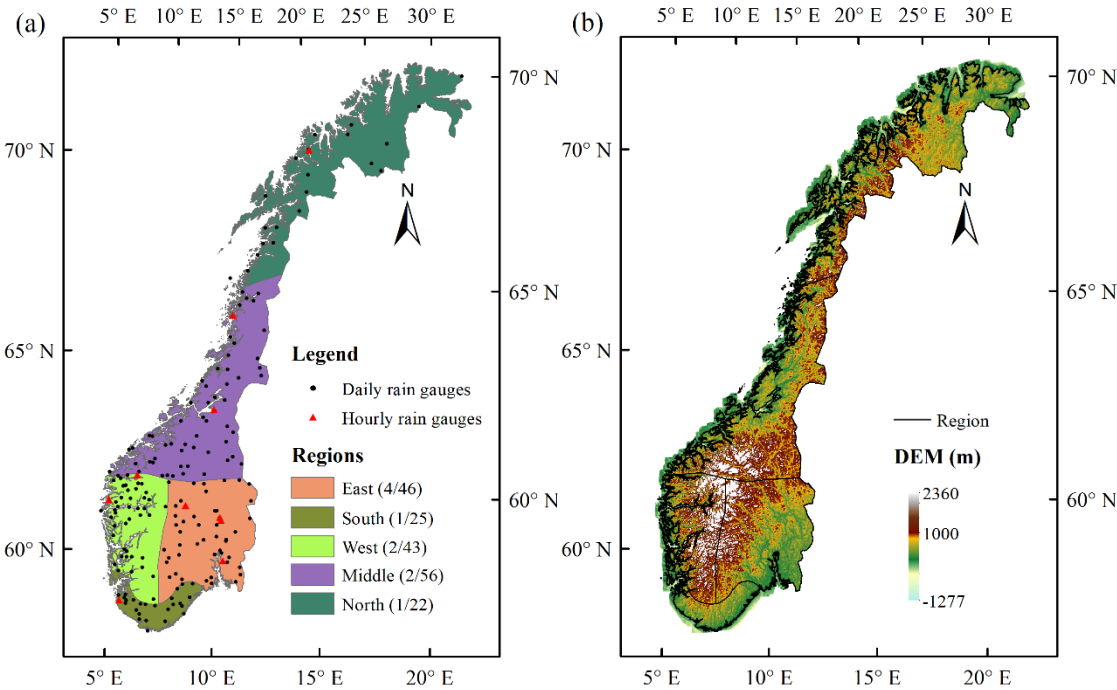
Figure 1: (a) The division of five regions in Norway. In the legend, the numbers shown in the brackets after each region represent the available size of hourly / daily stations in the region during 1999 – 2018. For example, East (4/46) means that there are available data from 4 hourly stations and 46 daily stations in the East during 1999-2018; (b) Spatial distribution of topography over Norway.

147

The different climate regimes between coastal and inland regions over Norway compels the analysis of hydro-meteorology based on divided regions. Based on similar seasonal cycle characteristics, Michel et al. (2021) and Konstali and Sorteberg (2022) divided the Norwegian continent into eight regions. Taking into account the spatial distribution of rain gauges and ensuring that each region has at least one hourly rain-gauge, we combined the south and southwest into the south, and the middle-inland and north into the north. Therefore, mainland Norway in this study is divided into five regions: East (E), South (S), West (W), Middle (M), and North (N), as shown in Fig. 1.

The study areas cover the mainland Norway which has unique climate characteristics within different regions. Precipitation in Norway primarily occurs along the coast in late autumn and winter, while inland areas receive more precipitation in summer. The eastern region with stratiform precipitation originating from south is dominant by continental climate, with convective precipitation in summer. The west coast of Norway is strongly affected by the North Atlantic storm track, where precipitation from frontal systems and landfalling storms is enhanced due to the orographic uplift over Scandinavia (Poujol et al., 2021). Most extreme events occurring in the western region with abrupt topography, are mainly related to atmospheric rivers (AR), which are generally linked to extratropical cyclones during cooler seasons (Whan et al., 2020). Additionally, in the summer, AR coincides with more frequent convective activities (Poujol et al., 2021). The southern region lies at the end of the climatological jet and is

163 regularly affected by the AR especially during the Zonal and Atlantic trough weather regimes (Michel et al., 2021),
164 while convective activities play a crucial role in the southern regions in summer (Li et al., 2020b). For the middle
165 and northern regions, 59% of extremes are associated with AR, and the precipitation rate decreases moving inland
166 (Konstali and Sorteberg, 2022).

167 **2.2 Data**

168 We utilize the outputs of double nested model simulations from the HCLIM38 model, which include different
169 configuration settings for each spatial resolution: HCLIM3 and HCLIM12. HCLIM12 covers most of Europe with
170 313 ×349 grid-points using the ERA-Interim reanalysis (~80 km) as the boundary condition, and HCLIM3 spans the
171 Fenno-Scandinavia region with 637×853 grid-points using the output of the HCLIM12 as the boundary condition for
172 every 3 h. Importantly, the convection-parameterization scheme was switched-off in HCLIM3, allowing for an
173 explicit representation of convection processes. The present-day simulations from HCLIM3 and HCLIM12 span the
174 years 1997-2018. For more comprehensive information, refer to the work of Lind et al. (2020) and Médus et al.
175 (2022).
176   This study primarily focuses on assessing the performance of HCLIM3 and HCLIM12 in simulating hourly
177 and daily extreme precipitation events in mainland Norway for the present-day period (1997-2018, with the first two
178 years excluded). The model outputs from HCLIM3 and HCLIM12 are specifically extracted for mainland Norway.
179 Before analysis, HCLIM3 data was remapped to the HCLIM12 grid (12km) using a bilinear interpolation method.
180   Precipitation from the seNorge2018 (SeNorge) gridded dataset, covering Norway with 1-day temporal and 1
181 km spatial resolution since 1957 (Lussana et al., 2019), is used as the observation dataset to evaluate the
182 performance of HCLIM3 and HCLIM12 during 1999-2018. Precipitation from the SeNorge2 gridded dataset, with
183 1-hour temporal and 1 km spatial resolution, is also applied to evaluate the hourly result during 2010-2018 (Lussana
184 et al., 2018). In addition, in-situ precipitation of observations, including both 1-hour and 1-day resolutions, are
185 downloaded from Norwegian Meteorological Institute Frost API (met.no).

186 **3 Methods**

187 **3.1 Evaluation of precipitation**

188 To evaluate the characteristics of precipitation extremes between HCLIM3 and HCLIM12, we compared the
189 historical simulations with daily SeNorge gridded dataset, hourly SeNorge2 gridded dataset and in-situ observations.
190 We only keep the stations that have less than 10% of the data missing during 1999-2018 and consider station
191 distribution uniformity, which give a total of 192 daily stations and 10 hourly stations, respectively, over Norway
192 (Fig. 1, Table S1 and Table S2). In this study, the evaluation based on in-situ observation and gridded dataset
193 (SeNorge and SeNorge2) was defined as the local scale and regional scale, respectively.
194   Remapping finer-resolution data to a coarser resolution reduces the influence of such artifacts by averaging out
195 the variability. This approach is consistent with the methodology used by Lind et al. (2020) and Médus et al. (2022),
196 who also remapped all data to a coarser grid when comparing the performance of HCLIM3 and HCLIM12. Lind et

al. (2020) observed that the differences between HCLIM3 data remapped to the coarser native grid of HCLIM3 and the HCLIM12 grid were minimal. Importantly, they found that the improvements of HCLIM3 persisted even after spatial aggregation, indicating that the enhanced resolution of the model offered benefits that were preserved when viewed on a coarser grid. Therefore, HCLIM3, SeNorge and SeNorge2 were remapped to HCLIM12 grid~12 km for the evaluation at regional scale. For the SeNorge and SeNorge2 based assessments, the extreme indices are first calculated at the grid-point level and then the regional averages are computed. For the evaluation based on in-situ observation, HCLIM3 and HCLIM12 were interpolated to the 192 daily rain-gauges and 10 hourly rain-gauges to calculate the indices using bilinear interpolation method.

For the evaluation of extreme precipitation, we examined the maximum 1-day precipitation (Rx1d), maximum 1-hour precipitation (Rx1h), return-period-based precipitation amounts at 5, 10, 20, and 50-year return periods, and seasonality of frequency/intensity from regional to local scales. The calculation of seasonal Rx1d/Rx1h was based on the maximum value within one season per year.

3.2 Extreme precipitation indices

The Generalized Extreme Value (GEV) distribution was used to estimate precipitation intensity for specific return periods (e.g., 5, 10, 20, and 50 years). The return levels were calculated by fitting the annual maximum discharge derived from observed and simulated daily data (both gridded and rain gauges), and hourly data (only 10 rain gauges), to GEV distribution. Then, the quantile Z_p of the GEV distribution with a return period of $\frac{1}{p}$ can be obtained. GEV distribution has been widely used to model extreme events in meteorology (Coles et al., 2003). The cumulative distribution function $F(x)$ and probability density function $f(x)$ of GEV were as follows to calculate the return level Z_p:

$$F(x) = exp\left\{-\left[1 - k\left(\frac{x-\xi}{\alpha}\right)\right]^{1/k}\right\}, k \neq 0 \tag{1}$$

$$f(x) = \frac{1}{\alpha}\left[1 - k\left(\frac{x-\xi}{\alpha}\right)\right]^{1/k-1} exp\left\{-\left[1 - k\left(\frac{x-\xi}{\alpha}\right)\right]^{1/k}\right\} \tag{2}$$

$$Z_p = \xi - \frac{\alpha}{k}\{1 - [-log(1-p)]^{-k}\} \tag{3}$$

Where, α, ξ, and k indicates the scale, location and shape parameter, respectively. Kolmogorov-Smirnovs, Anderson-Darlings, and Chi-Square tests were performed to determine if the GEV was accepted to fit the maxima series.

3.3 Quantification of the orographic effect

The orographic effect on Rx1h and Rx1d precipitation was explored by looking at the relationship with elevation of the annual and seasonal maxima from regional to local scales. A linear regression model (Di Piazza et al., 2011) was utilized to approximate the relations. The relationship of elevation with observation (Rx1h: SeNorge2; Rx1d: SeNorge and daily in-situ observation) and simulation (HCLIM3 and HCLIM12) was fitted to compute the linear

231 regression slope. To eliminate the impact of unit (Rx1h and Rx1d), the slope is transferred to relative slope with

232 respect to the average value of extreme precipitation, expressed as percentage precipitation (%) per kilometer of

233 elevation. The orographic effect at local scale was only based on daily in-situ observation due to the limited hourly

234 in-situ observation. At local scale, the elevation for each rain-gauges was extracted according to the digital elevation

235 model. At regional scale, the grid of digital elevation model and HCLIM3 was resample to the same grid resolution

236 of 12 km as HCLIM12 before calculation. Only the grids and stations above sea level of 0 m are included to

237 quantify the orographic effect.

238   If the precipitation increases with elevation, it means that the orographic effect on extreme precipitation; if the

239 precipitation decreases with elevation, its means that the reverse orographic effect on extreme precipitation.

240 **4 Results**

241 **4.1 Evaluation of daily extreme with SeNorge**

242 **4.1.1 Maximum 1-day precipitation (Rx1d)**

243
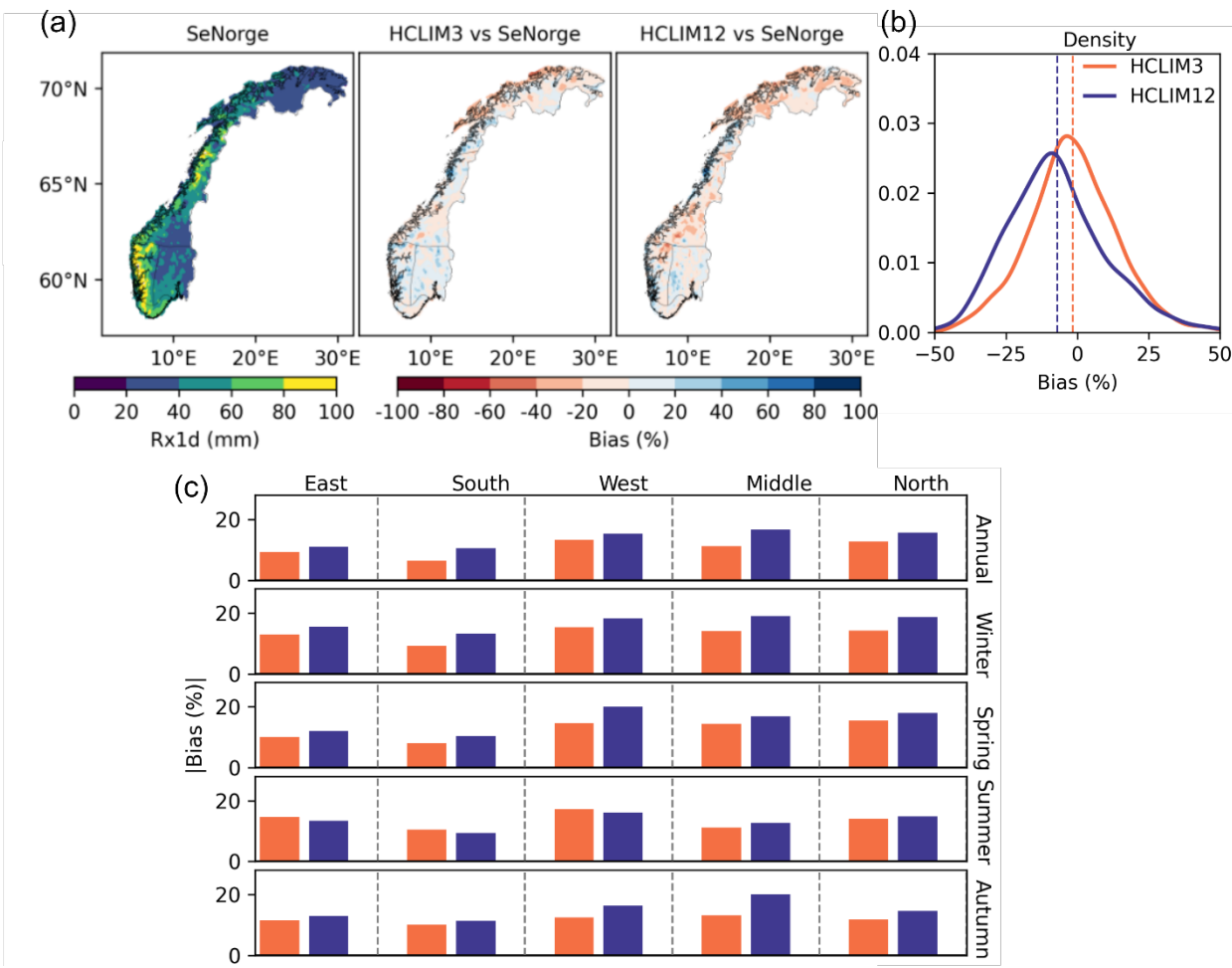
Figure 2: (a) The annual Rx1d of SeNorge, and the percentage bias **of Rx1d from HCLIM3 and HCLIM12 to SeNorge during 1999-2018; (b) density plot of the** percentage bias **distribution for** annual **Rx1d from HCLIM3 and HCLIM12 compared to SeNorge for Rx1d during 1999-2018** (The dashed lines represent the mean bias)**; (c) the** absolute percentage bias **of** annual and seasonal **Rx1d from HCLIM3 and HCLIM12 to SeNorge for five regions.** The bias is first calculated at the grid-point level, and then regional averages are computed. For (a) and (b), the percentage bias is equal to model simulations minus observations, divided by observations. For (c), the absolute percentage bias is calculated as the absolute difference between simulations and observations, divided by observations.

Figure 2 provides a comprehensive comparison of percentage biases of Rx1d from HCLIM3 and HCLMI12 compared to SeNorge. From Fig. 2 (a), we can see that HCLIM12 has more grids with underestimated Rx1d than HCLMI3 in Norway, which is confirmed clearly in Fig. 2 (b) showing density plot of the percentage bias distribution from two models compared with SeNorge. Specifically, more grids from HCLIM3 than HCLIM12 tend to overestimate Rx1d within the 0-25 % range, while HCLIM12 leans towards larger underestimation within the -10-50%. The density curve in Fig. 2 (b) reflects a higher peak at 0 for HCLIM3, indicating a more accurate representation of Rx1d with an average dry-bias with 1.6%. Conversely, HCLIM12 shows a 7% dry-bias for Rx1d on average.

   Figure 2 (c) shows the absolute percentage bias of annual and seasonal Rx1d from HCLIM3 and HCLIM12 compared to SeNorge for five regions in four seasons. In annual, HCLIM3 exhibit added value in capturing annual Rx1h in the five regions compared to HCLIM12. HCLIM3 better captures Rx1d in four seasons and annual for five regions than HCLIM12, while HCLIM12 shows larger bias in most regions except in the east, south and west during summer. In summer, HCLIM3 only outperforms Rx1d in the middle and north over HCLIM12. Overall, HCLIM3 shows notably added value in Rx1d comparing with HCLMI12 across regions and seasons except in summer.

   Furthermore, as shown in Fig. 3, a comparison of the Rx1h percentage biases of HCLIM3 and HCLIM12 with SeNorge2 for the period 2010-2018 demonstrates that HCLIM3 has a clearly added value in simulating the annual Rx1h in Norway, with smaller wet biases on average, while HCLIM12 shows larger dry biases over the whole of mainland Norway. At the regional scale, HCLIM3 also shows added value in capturing annual and seasonal Rx1h than HCLIM12 in five regions except west and middle regions. Specifically, in the west region, HCLIM3 exhibits larger absolute percentage biases than HCLIM12 in annual Rx1h and seasonal Rx1h than HCLIM12, except in spring. In summer, only in the south and north regions, the Rx1h bias of HCLIM3 is smaller than that of HCLIM12.
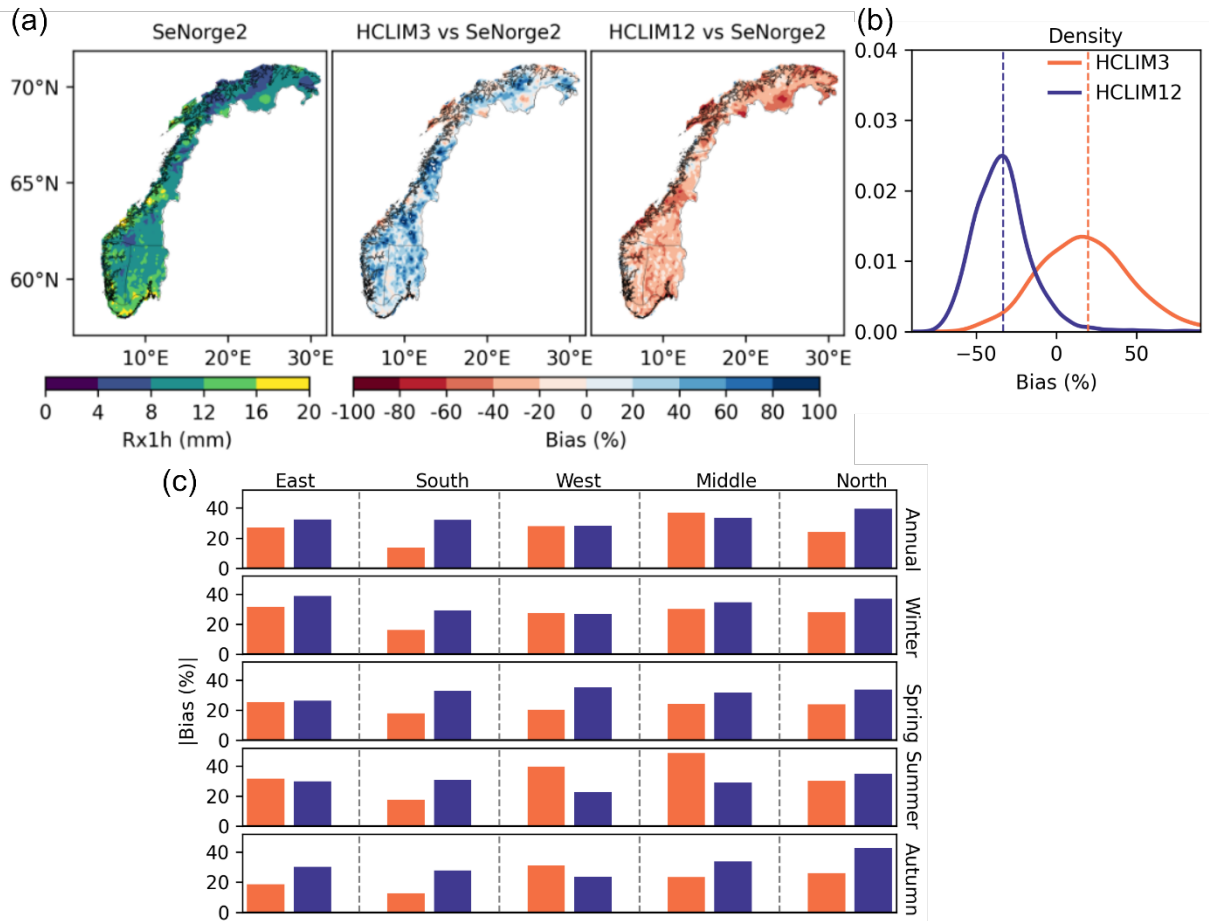
Figure 3: (a) The annual Rx1h of SeNorge2, and the percentage bias of Rx1h from HCLIM3 and HCLIM12 to SeNorge2 during 2010-2018; (b) density plot of percentage bias for annual Rx1h distribution from HCLIM3 and HCLIM12 compared to SeNorge2 during 2010-2018 (The dashed lines represent the mean bias); (c) the absolute percentage bias of seasonal Rx1h from HCLIM3 and HCLIM12 to SeNorge2 for five regions. For (a) and (b), the percentage bias is equal to model simulations minus observations, divided by observations. For (c), the absolute percentage bias is calculated as the absolute difference between simulations and observations, divided by observations.

4.1.2 Return levels

Figure 4 shows the bias in estimated daily precipitation for 5-, 10-, 20-, and 50-year return periods during 1999-2018 across five regions (compared to SeNorge). The great interregional variation is shown between HCLIM3 and HCLIM12. Relative to SeNorge, HCLIM3 tends to overestimate return-levels in the eastern and western regions, while underestimates them in the others. By comparison, except for the east region where HCLIM12 shows overestimation, the extreme precipitation estimates in most other regions are underestimated. The performance of HCLIM3 in capturing extremes varies across regions. HCLIM3 and HCLIM12 exhibit percentage biases of opposite sign in simulating return level precipitation in the western region, where HCLIM3 overestimates and HCLIM12 underestimates precipitation at different return periods. In the western, middle, and northern regions, HCLIM3 outperforms HCLIM12 in all return periods, but the performance is less satisfactory in the eastern region.

291   Given the societal impacts of precipitation extremes, understanding how HCLIM3 and HCLIM12 represent

292   these extremes is crucial. The physical processes driving precipitation in inland and coastal regions, as highlighted

293   by Konstali and Sorteberg (2022), emphasize the need for a separate evaluation for each region with different

294   characteristics. This approach ensures a more robust assessment, providing valuable information for regional

295   authorities.
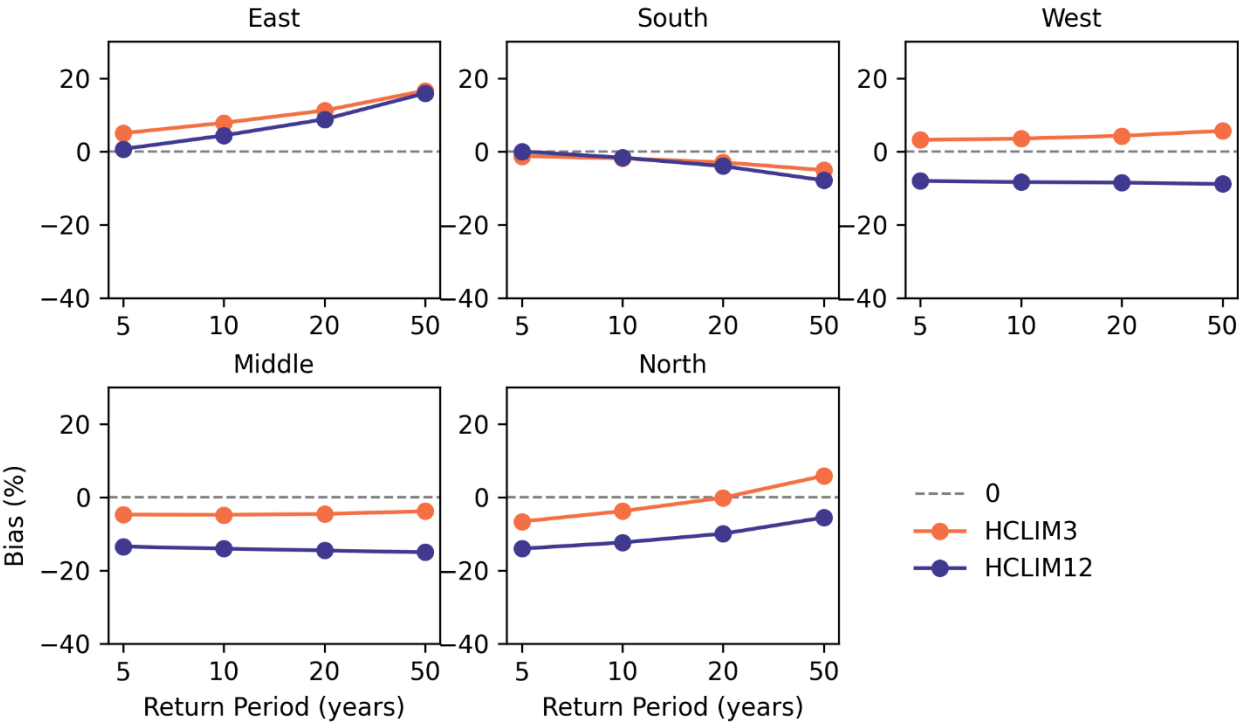
296
297   **Figure 4: Percentage bias of extreme daily precipitation exceeding the 5-year to 50-year return periods over five regions**
298   **between SeNorge and HCLIMs (i.e., HCLIM3 and HCLIM12). Return periods of 5-, 10-, 20-, and 50-year are calculated**
299   **on the basis of GEV.**

4.2 Evaluation of daily extreme with in-situ data

4.2.1 Maximum 1-day precipitation (Rx1d)
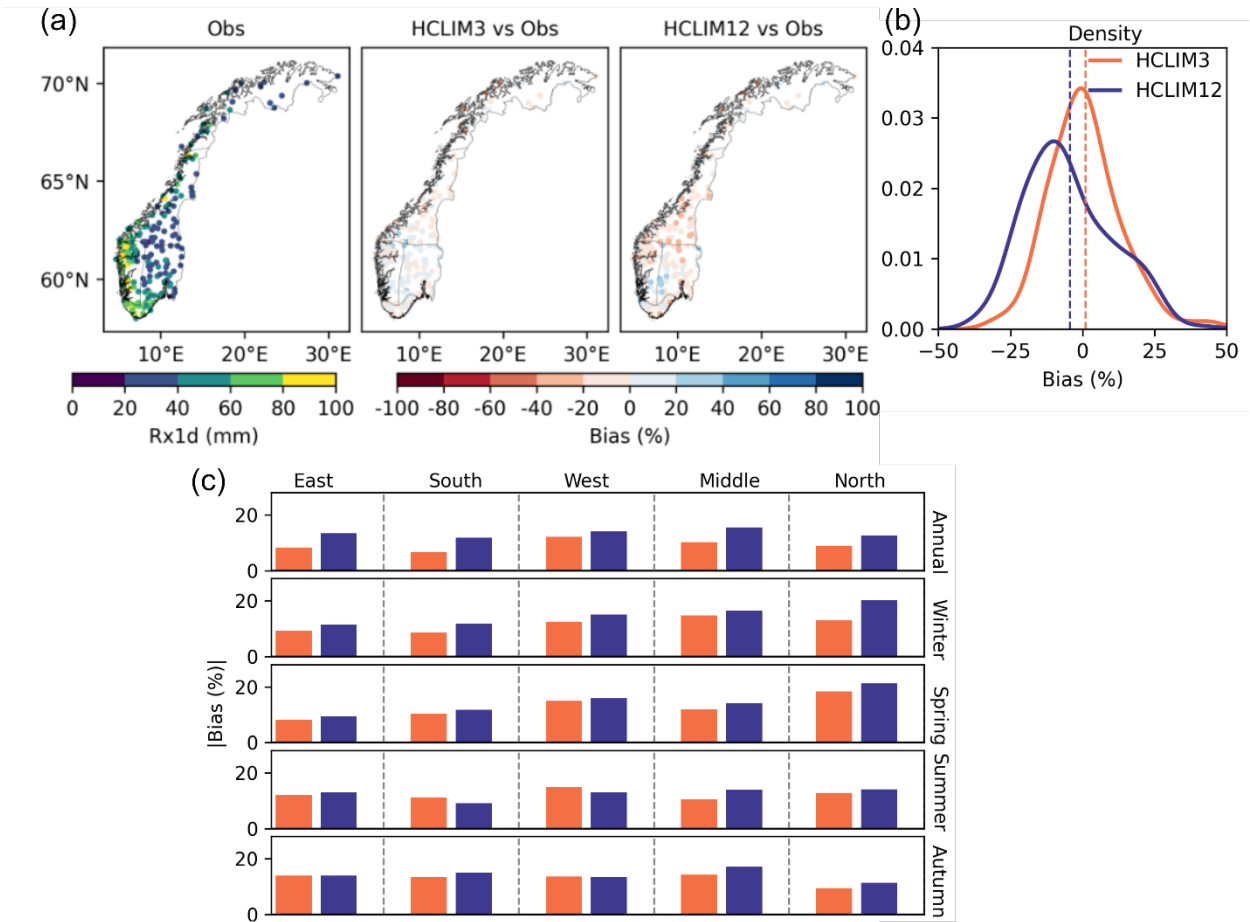
Figure 5: (a) The annual Rx1d of in-situ observation, and the percentage bias of Rx1d from HCLIM3 and HCLIM12 to in-situ observation during 1999-2018 over 194 stations; (b) density distribution of percentage bias for annual Rx1d between HCLIMs and observations from 194 stations during 1999-2018 (The dashed lines represent the mean bias); (c) the absolute percentage bias of seasonal Rx1d between HCLIMs and observations across the five regions. For (a) and (b), the percentage bias is equal to model simulations minus observations, divided by observations. For (c), the absolute percentage bias is calculated as the absolute difference between simulations and observations, divided by observations.

Similar to the regional results in Fig. 2, Fig. 5 shows the percentage bias of annual and seasonal Rx1d from HCLIM3 and HCLIM12 in comparison to in-situ observations. Notably, a difference between HCLIM3 and HCLIM12 can be seen at local scale compared to regional result: a greater number of sites from HCLIM3 approach zero-bias, and more grids from HCLIM12 shows a dry bias about 10-40%, as shown in Fig. 5 (b). On average, HCLIM12 with 4.5% dry-bias tends to underestimate annual Rx1d, while HCLIM3 represents added value in capturing annual Rx1d with 1% wet-bias on average at local scale. Furthermore, HCLIM3 shows added value in simulating the annual Rx1h at local scale in all regions.

From a seasonal perspective, as shown in Fig. 5 (c), overall, HCLIM3 shows added value in capturing the seasonal Rx1d in most regions and seasons, except for summer. Specifically, HCLIM3 performs better than

319   HCLIM12, except for the western and southern region, where HCLIM3 exhibits a larger bias in summer Rx1d. In

320   particular, the added value of HCLIM3 in simulating autumn Rx1d in the east and west is not as obvious when

321   compared to HCLIM12.

322   It is noteworthy that at the local scale, HCLIM3 and HCLIM12 perform similarly to the regional results in most

323   regions. There are some exceptions, such as, HCLIM3 shows larger biases in summer Rx1d in the south and west

324   compared with HCLIM12 at both regional and local scales. In contrast to the clearly larger bias in Rx1h at the

325   regional scale for both HCLIM3 and HCLIM12, a relatively smaller bias in Rx1d is demonstrated at both regional

326   and local scales. At the regional scale, HCLIM3 exhibits added value in all seasons except summer, while at the

327   local scale, HCLIM3 and HCLIM12 show similar biases in autumn Rx1d in the east and west, which means that the

328   advantage of HCLIM3 over HCLIM12 at the local scale in autumn weakens in the west and east compared with the

329   regional scale.

330   **4.2.2 Return-levels**

331
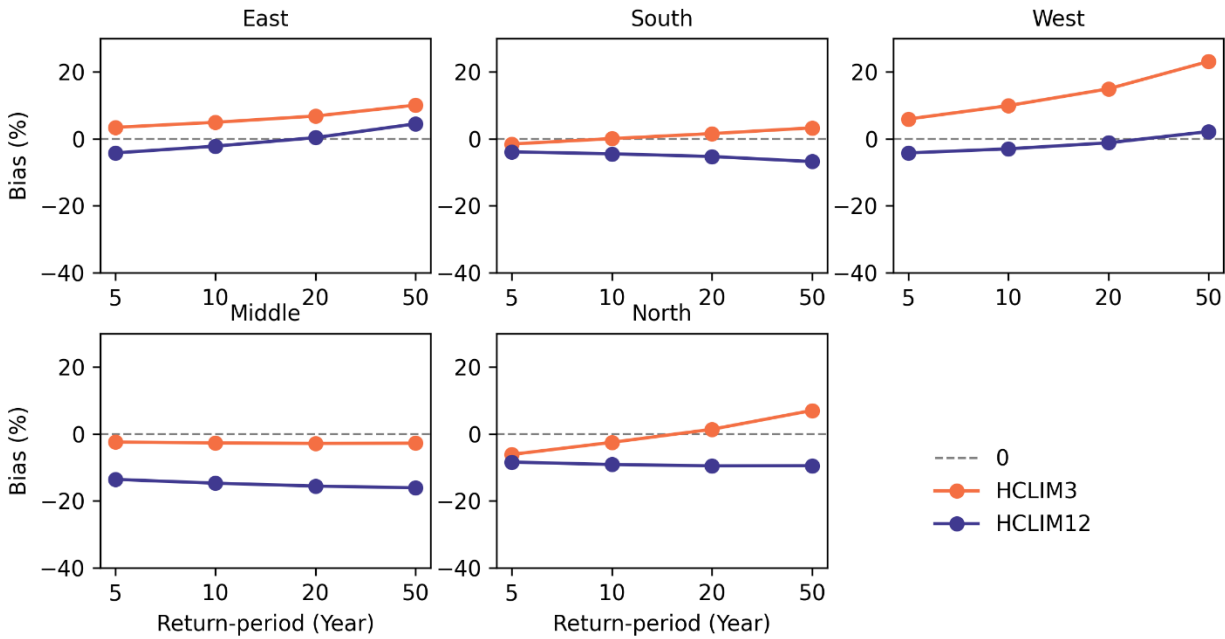
332   **Figure 6: Percentage bias of extreme daily precipitation exceeding the 5-year to 50-year return periods over five regions**
333   **between HCLIMs (i.e., HCLIM3 and HCLIM12) and in-situ observation in the 192 daily rain-gauges. Return periods of**
334   **5-, 10-, 20-, and 50-year are calculated on the basis of station-scale GEV.**

335

336   Figure 6 shows the percentage bias of the estimated daily return levels (e.g., 5-, 10-, 20-, and 50-year return periods)

337   from HCLIM3 and HCLIM12 compared to observations for the period 1999-2018. The figure illustrates the average

338   bias of return-levels for the stations in the corresponding regions. Compared with the in-situ observation, HCLIM3

339   overestimates the return levels in the east and west for all return periods (5-, 10-, 20-, and 50-year) and

340   underestimates return levels in the south and north for 20- and 5-year return periods, while HCLIM12

341   underestimates the return levels in all regions. Generally, HCLIM3 can more accurately represent the return levels in

342   most regions compared to HCLIM12. The biases of HCLIM3 and HCLIM12 vary across regions and return periods.

343 HCLIM3 has lower biases than HCLIM12 in most regions, except for the eastern and western regions. Both

344 HCLIM3 and HCLIM12 perform well in the southern region. In addition, Fig. S1 shows the range of the return

345 levels for all stations in the corresponding region, and HCLIM3 introduces larger variations in the western and

346 southern regions compared with HCLIM12, as indicated by the wider whiskers.

347 **4.3 Evaluation of hourly extreme with in-situ data**

348 **4.3.1 Maximum 1-hour precipitation (Rx1h)**

349 The time evolution of annual Rx1h from HCLIM3 and HCLIM12 is compared to in-situ observation during 1999-

350 2018, as shown in Fig. 7. Compared to HCLIM12, HCLIM3 shows distinct superior in capturing the time evolution

351 of annual Rx1h, even with underestimation and time shifting at some local places. For example, the annual Rx1h

352 above 25 mm/hour at Kvithamar (SN69150), Særheim (SN44300), Tromsø - Holt (SN90400), Tjøtta (SN76530) and

353 Løken i Volbu (SN23500) is struggle to be captured by HCLIM3 and HCLIM12. However, HCLIM3 well capture

354 the annual Rx1h in other local places, despite of the time deviation of annual Rx1h. Taking the site Østre Toten -

355 Apelsvoll (SN11500) as an example to illustrate the time deviation: HCLIM3 simulate that the annual Rx1h (37

356 mm) in the past 20 years was in 2001, four years earlier than the in-situ observation (35 mm). Furthermore, to better

357 assess the annual variability of Rx1h, we extracted grids within a 12 km radius of each station and calculate the

358 uncertainty range (Fig. S2), which reveals that the interpolated local Rx1h precipitation from HCLIM12, particularly

359 over grids with a larger area, tends to be damped, resulting in a narrower range than HCLIM3. Based on station

360 statistics of annual mean Rx1h in Norway, the boxplot (Fig. 7) shows that the annual mean Rx1h of HCLIM3 is

361 within the range of observed values. In contrast, HCLIM12 consistently underestimates Rx1h, with all its values

362 being below the observed minimum. Despite outperforming than HCLIM12, it is noteworthy that HCLIM3

363 demonstrates limitations in reproducing the accurate occurrence time and magnitude of annual Rx1h at local-level in

364 Norway.

365

366
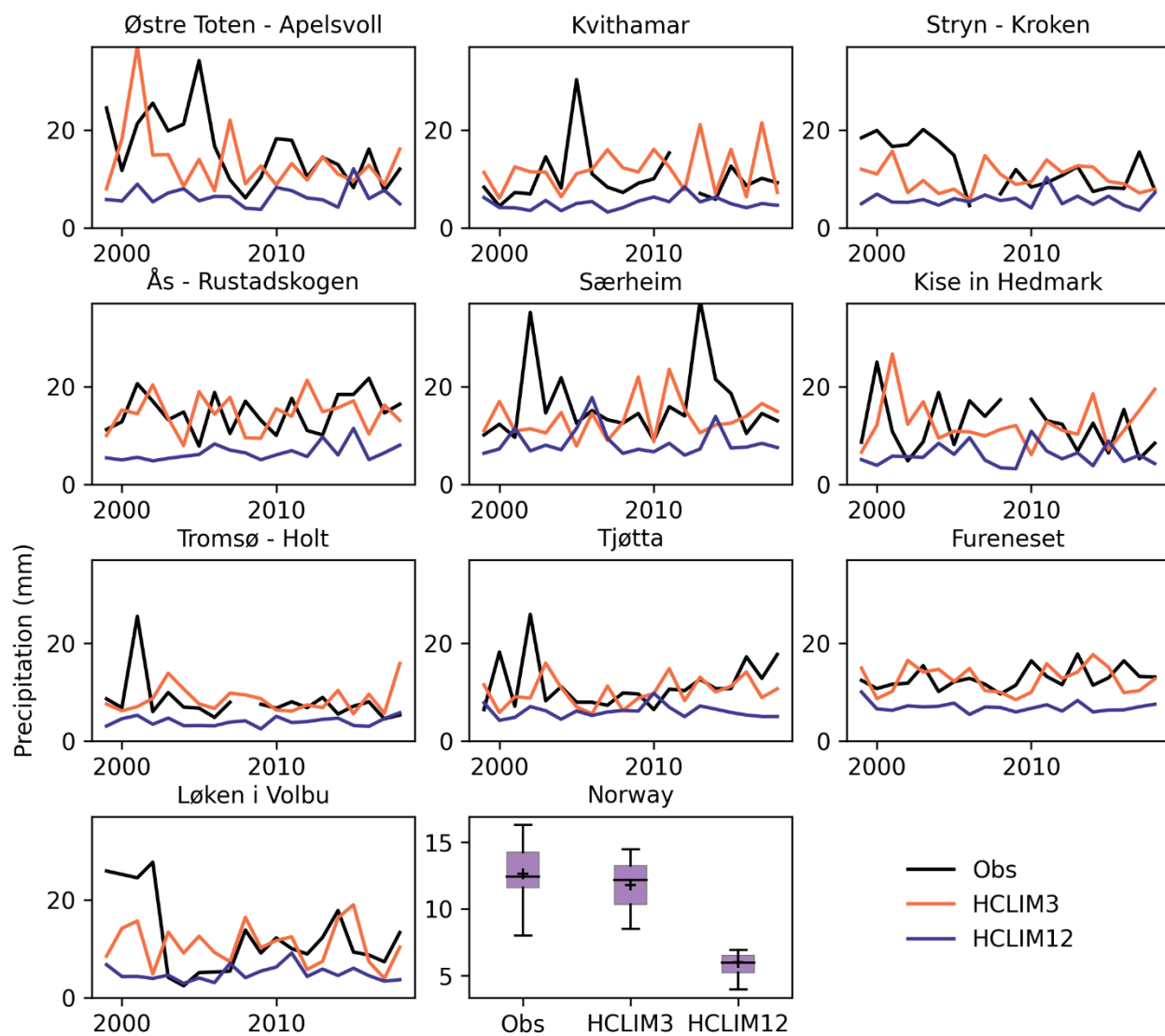
Figure 7: Time evolution of Rx1h precipitation for each year from observation, HCLIM3 and HCLIM12 during 1999-
2018 at 10 rain-gauges (Table S1).

369

4.3.2 Return levels
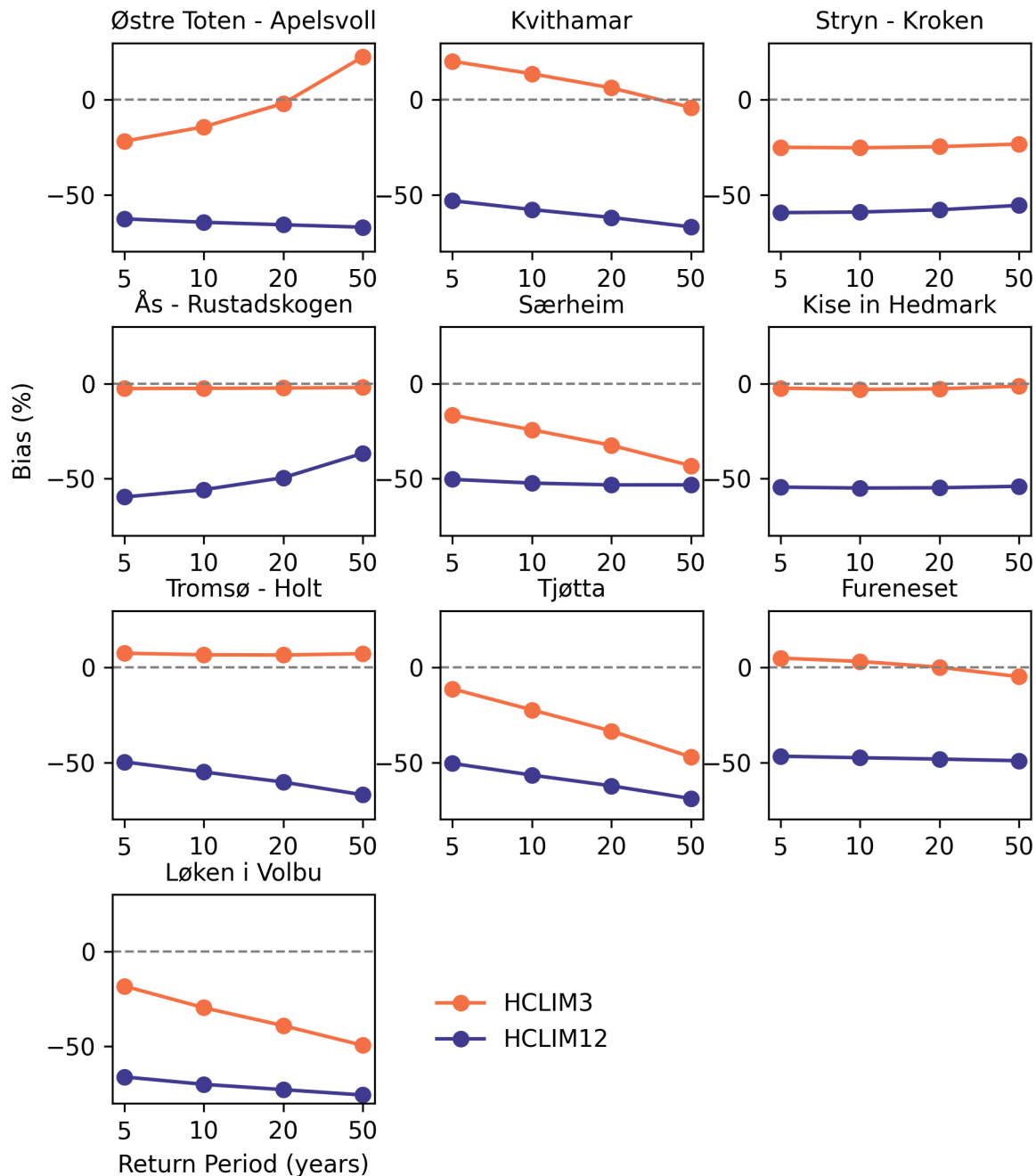
Figure 8: Percentage bias of extreme hourly precipitation exceeding the 5-year to 50-year return periods between HCLIMs (i.e., HCLIM3 and HCLIM12) and in-situ observation in the 10 hourly rain-gauges. Return periods of 5-, 10-, 20-, and 50-year are calculated on the basis of station-scale GEV.

At the local and hourly scale, HCLIM3 has a better representation of hourly extreme events at the 5-, 10-, 20-, and 50-year return periods compared to HCLIM12. Although both HCLIM3 and HCLIM12 tend to underestimate the annual Rx1h for all return periods at almost stations (Fig. 8), the biases between the observations and the

380 interpolated HCLIM3 for all ten rain gauges are consistently lower than those of HCLIM12 for all return periods.

381 The exceptions are Kvithamar (SN69150), Tromsø - Holt (SN90400) and Fureneset (SN56420) which present at all

382 return periods, and Østre Toten - Apelsvoll (SN11500) which present at a 50-year return period, where HCLIM3

383 slightly overestimation. Notably, the return levels of hourly extreme events at all ten sites are accurately captured by

384 HCLIM3, demonstrating its better ability to capture the extreme hourly precipitation at the 5-, 10-, 20-, and 50-year

385 return periods in localized areas, compared to HCLIM12. This result underscores the added value of CPRCMs in

386 representing hourly extreme precipitation at a very localized scale, despite the overall underestimation of return

387 levels by both HCLIM3 and HCLIM12.

388 **4.4 Evaluation of seasonality**

389
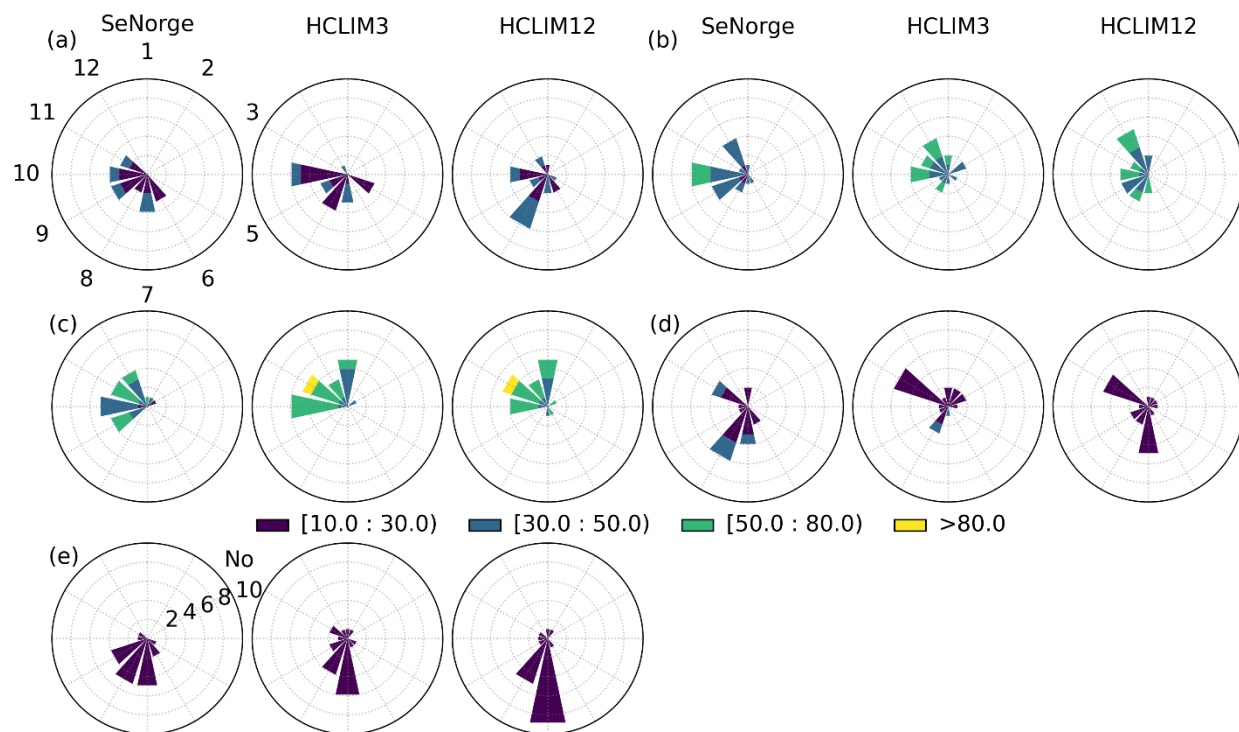
390 **Figure 9: The seasonality of frequency and magnitude of Rx1d precipitation from the SeNorge, HCLIM3 and HCLIM12**
391 **during 1999-2018 over different regions: a) Eastern, b) South, c) West, d) Middle, f) North. The color represents the**
392 **magnitude of Rx1d (m³/s). Winter: December, January, February; Spring: March, April, May; Summer: June, July,**
393 **August; Autumn: September, October, November.**

394
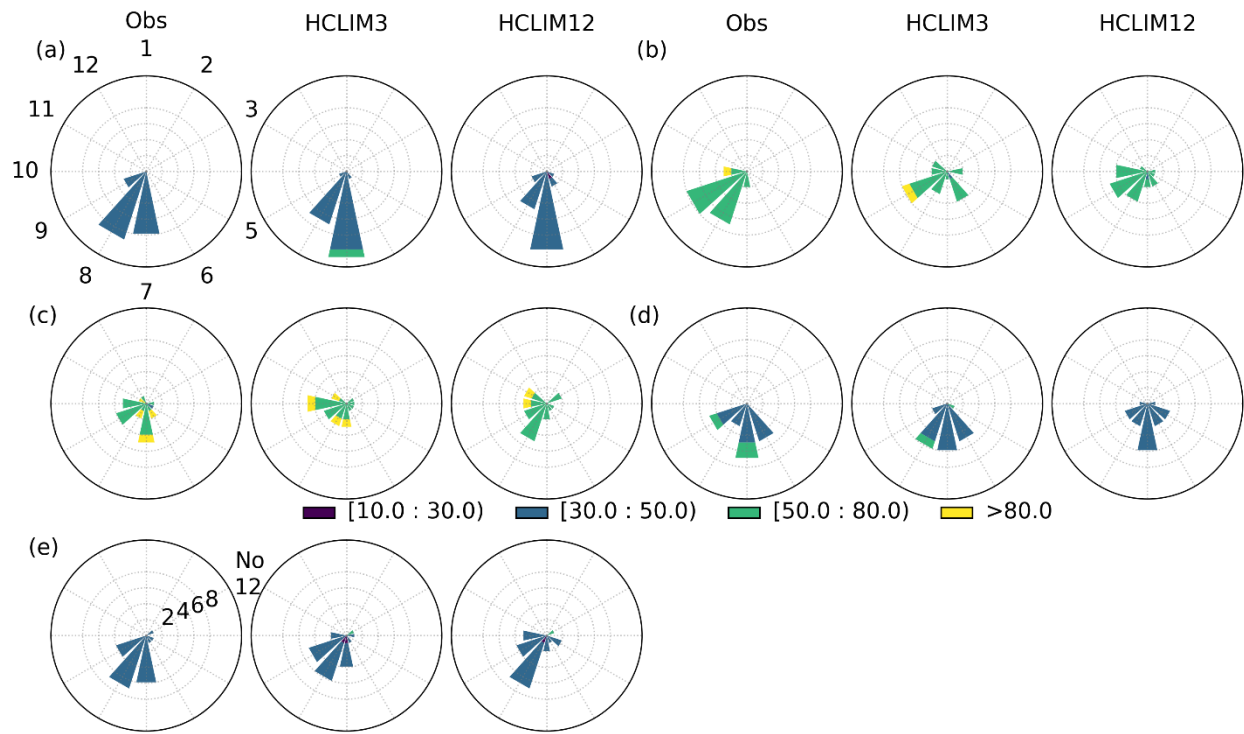
Figure 10: The seasonality of frequency and magnitude of Rx1d precipitation from the in-situ observation, HCLIM3 and
HCLIM12 during 1999-2018 over different regions: a) Eastern, b) South, c) West, d) Middle, f) North. The color
represents the magnitude of Rx1d (m^3/s).

398
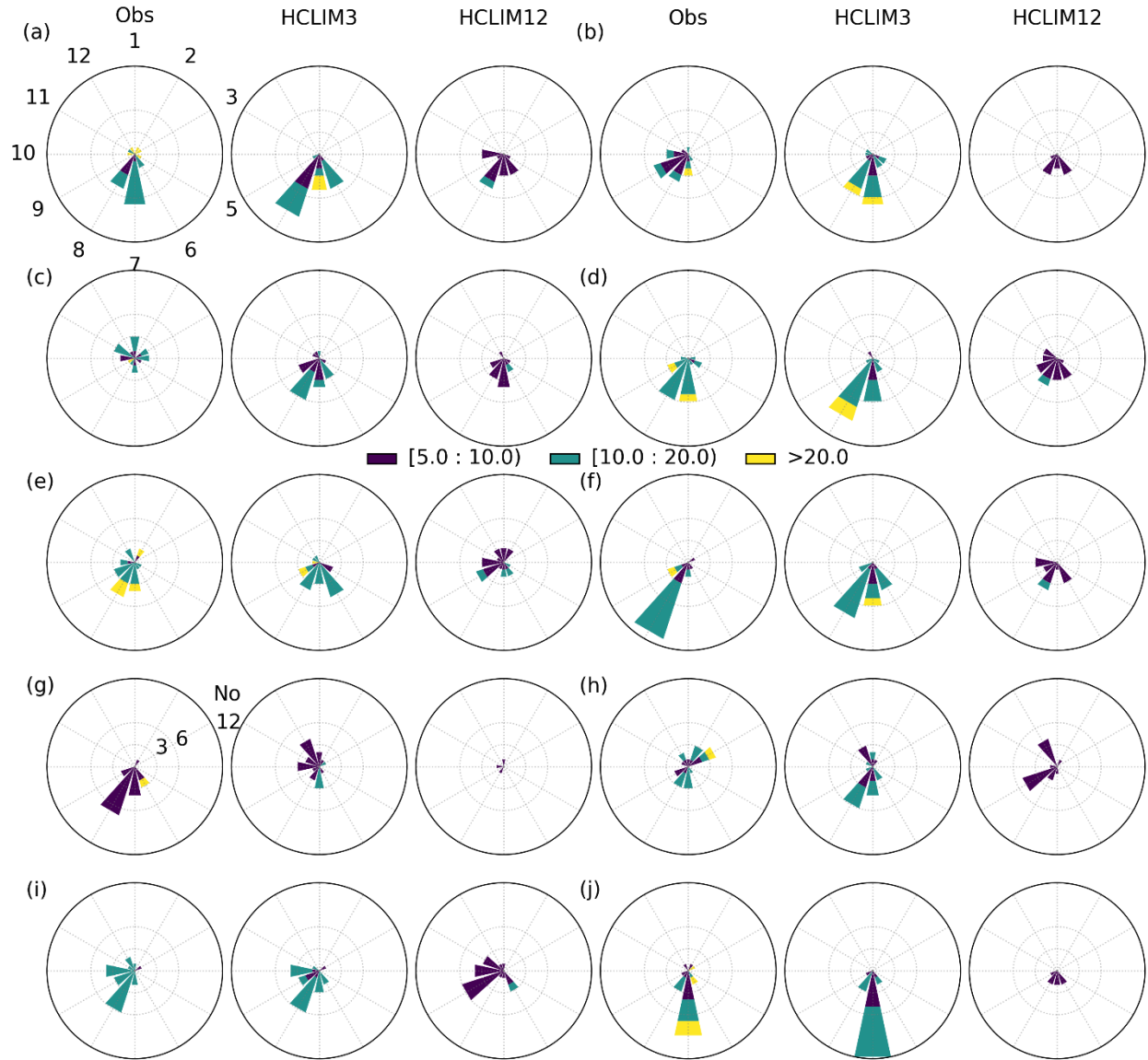
Figure 11: Seasonality of the frequency and magnitude of Rx1h precipitation from the in-situ, HCLIM3 and HCLIM12 during 1999-2018 at 10 rain gauge stations (Table S1), i.e., a) Østre Toten - Apelsvoll, b) Kvithamar, c) Stryn - Kroken, d) Ås - Rustadskogen, e) Særheim, f) Kise in Hedmark, g) Tromsø – Holt, h) Tjøtta, i) Fureneset, j) Løken i Volbu. The color represents the magnitude of Rx1h (m³/s).

Figure 9 and Figure 10 show the comparison of seasonality (indicated by monthly distribution) of annual Rx1d (e.g., frequency and magnitude) from both HCLIM3 and HCLIM12, compared to SeNorge and in-situ observation, respectively. From the seasonality of observed daily extreme precipitation in Fig. 9, we can see that winter-autumn precipitation dominates in almost all regions, except the middle and northern regions, where spring-summer precipitation is more prevalent. HCLIM3 captures the seasonality of Rx1d frequency at the regional scale in most regions except in middle region, where winter-autumn precipitation dominates. In contrast, HCLIM12 performs poorly in the eastern and middle regions. It is particularly noteworthy that HCLIM3 has an enhanced ability to capture the seasonality of extreme precipitation frequency over the western region compared to HCLIM12. Heavy

413 precipitation over 50 mm/day occurs mainly in the south and west, which is also simulated by HCLIM3 and

414 HCLIM12. In general, both HCLIM3 and HCLIM12 demonstrate competence in capturing the magnitude of

415 extreme daily precipitation seasonally at regional scale in most regions except middle region.

416   The seasonal performance of Rx1d from HCLIM3 and HCLIM12 in the local scale is also confirmed by the in-

417 situ observation, as shown in Fig. 10. A larger magnitude of annual Rx1d across five regions at local scale than

418 regional scale is shown for observation, HCLIM3 and HCLIM12. Generally, spring-summer precipitation events are

419 more frequent in the east, middle and north, while winter-autumn events are frequent in the south and west, and both

420 HCLIM3 and HCLIM12 capture this pattern well. In comparison, HCLIM3 better represents the seasonality of

421 frequency in the south, west and middle, compared to HCLIM12. For the seasonality of annual Rx1d at local scale,

422 as shown in Fig. 11, HCLIM3 more accurately represents the seasonality of Rx1h compared to HCLIM12, which

423 tends to underestimate the frequency of hourly extremes in most sites. Compared with RCMs, CPRCMs demonstrate

424 better potential performance in simulating seasonality of extreme precipitation, with particularly improved accuracy

425 for the hourly extremes at the local scale.

4.5 Orographic effect on seasonal extreme precipitation

4.5.1 Seasonal Rx1d at regional scale
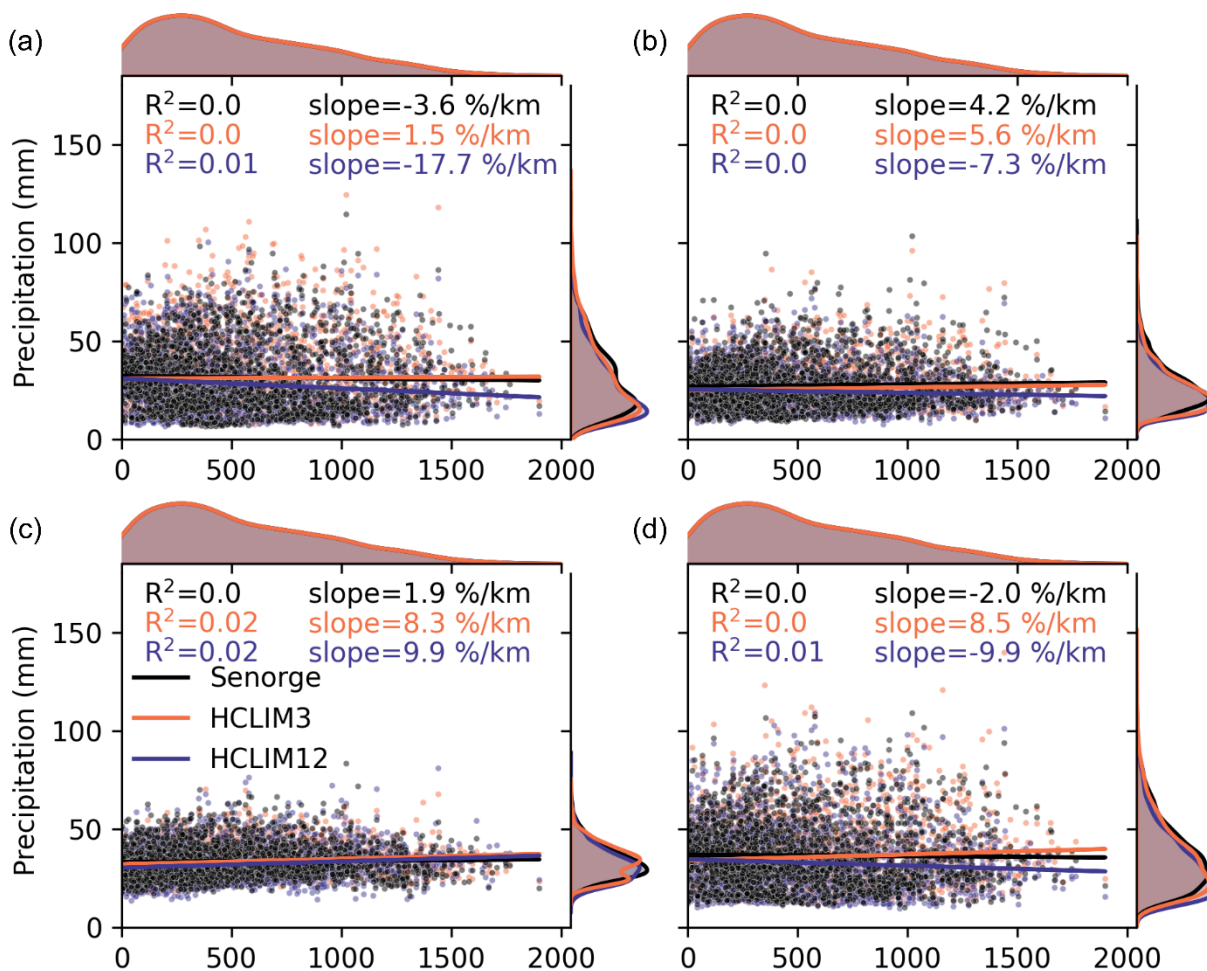
Figure 12: Relationship between elevation and Rx1d (maximum 1-day precipitation) for (a) winter, (b) spring, (c) summer, and (d) autumn, as derived from SeNorge and HCLIMs (i.e., HCLIM3 and HCLIM12) across mainland Norway during the period of 1999-2018.

The relationship of seasonal Rx1d with elevation from SeNorge, HCLIM3 and HCLIM12 is shown in Fig. 12. Compared to HCLIM12, HCLIM3 more accurately captures the no evident linear relation (indicated by zero coefficient of determination R^2) of seasonal Rx1d with elevation, similar to SeNorge, though it depicts a more pronounced increase with elevation than SeNorge during summer. For example, both HCLIM3 and HCLIM12 simulate a large average increase in summer Rx1d with elevation (over 8 %/km, compared to observation), as indicated by the larger absolute slope values. Generally, SeNorge, HCLIM3 and HCLIM12 showed the weak relationship of seasonal Rx1d with altitude.

 4.5.2 Seasonal Rx1d at local scale

441
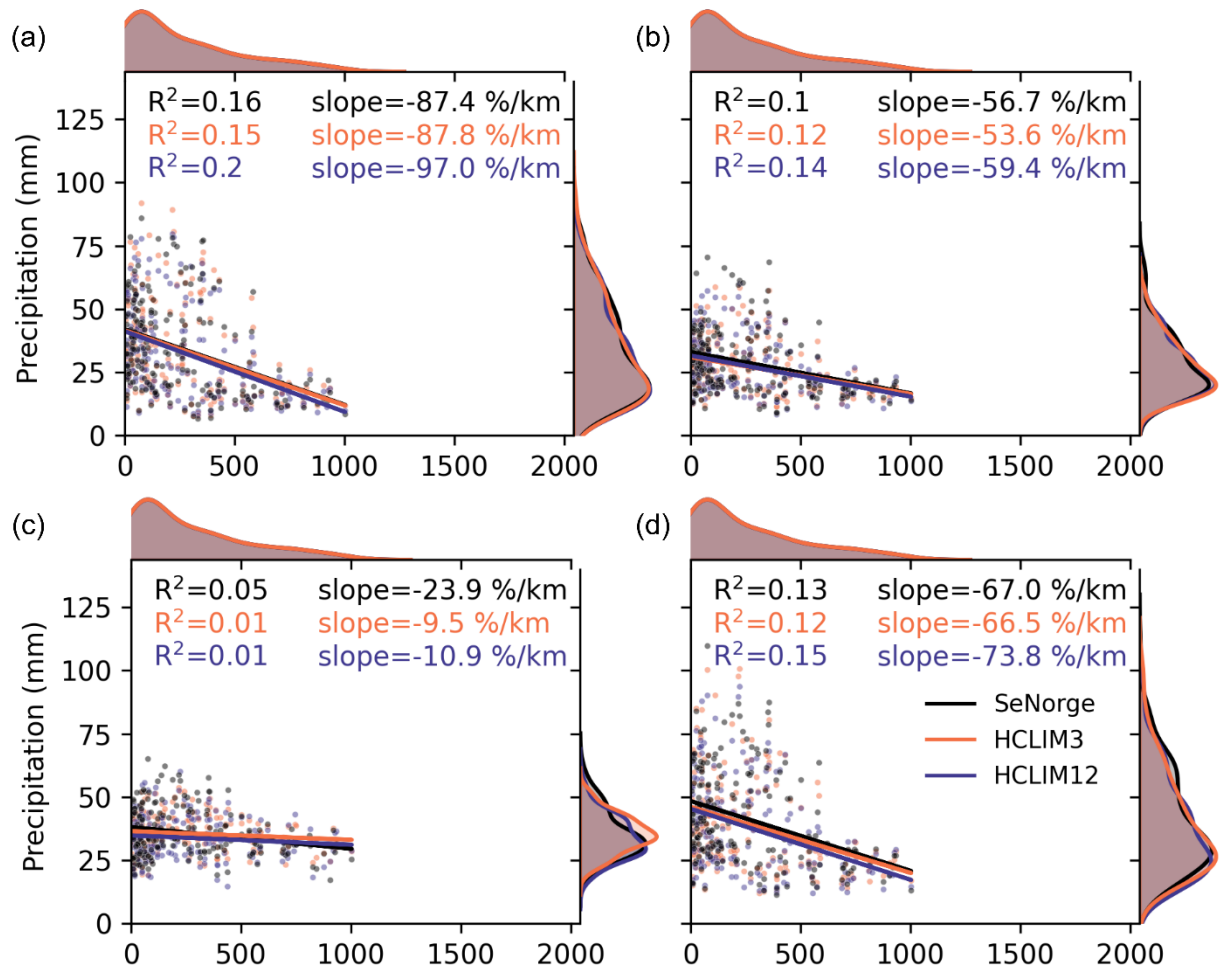
Figure 13: Relationship between elevation and Rx1d (maximum 1-day precipitation) for (a) winter, (b) spring, (c) summer, and (d) autumn, based on daily in-situ observation and HCLIMs (i.e., HCLIM3 and HCLIM12) across mainland Norway during the period of 1999-2018.

445

446   Figure 13 represents the relationship of the seasonal Rx1d from in-situ observation, HCLIM3 and HCLIM12 with

447   elevation at local scale. The observed reverse orographic effect, seasonal Rx1d decrease with elevation, clearly

448   depicts with an average decrease of winter, spring, summer and autumn Rx1d of more than 87.4%, 56.7%, 23.9%

449   and 67% per kilometer. HCLIM3 more accurately represents the observed orographic influences on Rx1d in all

450   seasons except summer than HCLIM12. Moreover, HCLIM12 displays a more pronounced decline in Rx1d with

451   elevation, as evidenced by a steeper slope, across all seasons except summer, when compared to observation.

452   Generally, the reverse orographic effect is shown for the Rx1d from in-situ observation, HCLIM3 and HCLIM12.

4.5.3 Seasonal Rx1h at regional scale
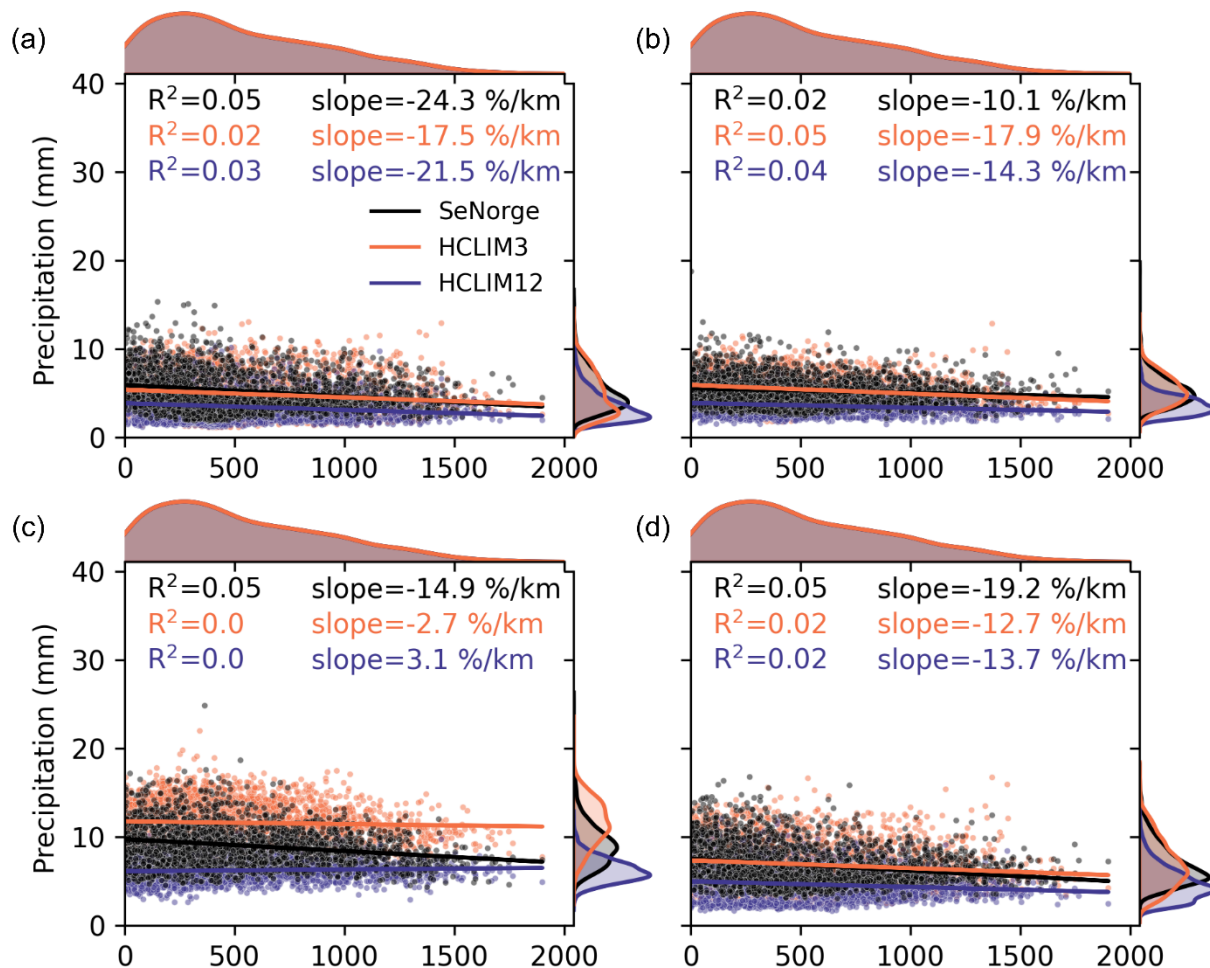
Figure 14: Relationship between elevation and Rx1h (maximum 1-hour precipitation) for (a) winter, (b) spring, (c) summer, and (d) autumn, as derived from SeNorge2 and HCLIMs (i.e., HCLIM3 and HCLIM12) across mainland Norway during the period of 2010-2018.

The relationship of seasonal Rx1h with elevation from gridded observation (SeNorge2) and simulation is further explored, as shown in Fig. 14. The reverse orographic effect of SeNorge2 on Rx1h was manifested in all seasons, with average decreases exceeding 24.3%, 10.1%, 14.9% and 19.2% per kilometer in winter, spring, summer and autumn, respectively. Compared to HCLIM12, HCLIM3 more accurately captures the decrease in seasonal Rx1h with elevation during winter, summer and autumn, though it still underestimates the decrease rate relative to observation. By contrast, HCLIM12 can only reflect the similar reverse orographic on Rx1h with observation in spring. The density plots of Rx1h reveal a dry bias in HCLIM12, particularly noticeable in summer, where it inversely correlates Rx1h with elevation.

5 Discussion

     5.1 Comparison between SeNorge vs in-situ observation
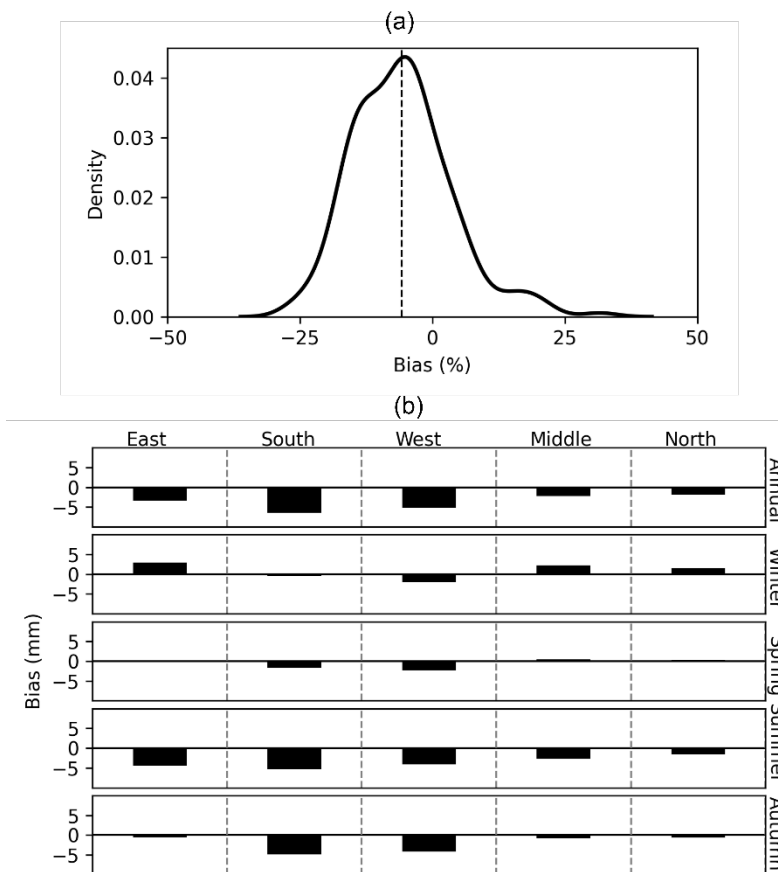
Figure 15: (a) Density distribution of bias for Rx1d between SeNorge and daily in-situ observations from 194 stations during 1999-2018; (b) the percentage difference of seasonal Rx1d between SeNorge and daily in-situ observations across the five regions. The bias is calculated as the SeNorge minus daily in-situ observations at each grid-point.

To further explore the uncertainty of different observation datasets on local scale model evaluation, we investigate the bias of SeNorge's annual and seasonal Rx1d from daily in-situ observations (see in Fig. 15). Our analysis in the Fig.15 (a) shows that SeNorge mostly underestimates the annual Rx1d compared to in-situ observation at 192 stations, with an average bias of -5.8% and a range between -28% and 25%. Although SeNorge data are designed to improve hydrological simulations (Lussana et al., 2019), their dry-biases still persist in most seasons and regions, especially in summer. It is noteworthy that SeNorge slightly overestimates the winter Rx1d in eastern, middle and northern regions. Moreover, SeNorge underestimates the return levels of Rx1d for different return periods (e.g., 5-, 10-, 20- and 50-year) in all regions (Fig. S3).

The larger differences between SeNorge and in-situ observation in simulating the Rx1d are manifested in the annual summer and autumn in the south and west, and in the summer in the east, where SeNorge tends to underestimate Rx1d more than in-situ observation. This discrepancy helps explain the differences between HCLIM3's performance in simulating Rx1d in summer in the east and autumn in the south and west at regional scale, compared to the local scale, as shown in Fig. 2 (c) and Fig. 5 (c). Generally, the difference between SeNorge

and in-situ observation at daily scale is not very large, which is why in most regions the added value of HCLIM3 in Rx1d at the regional scale is similar to that at the local scale. However, it should be noted that the interpolated precipitation from SeNorge may introduce uncertainties in assessing the performance of CPRCM at the local scale due to the sparse distribution of daily and hourly rain-gauges at high altitude. Especially, for the hourly extremes at the local scale and regional scales, larger uncertainties should be considered due to the limited data from only ten rain-gauges at local scales and nine-years of data series at the regional scale. The impact of station density on the errors of gridded datasets were also highlighted by Gervais et al. (2014b), who suggested that low station density is an important source of errors in such datasets. To address these challenges and enhance the accuracy of extreme precipitation assessments, future studies should prioritize expanding in-situ datasets and improving the spatial coverage of observational networks, especially at the 1-hour timescale.

5.2 Added value of CPRCMs at regional scale

HCLIM3 demonstrates clear advantages over HCLIM12 in capturing the annual Rx1d in most regions. In terms of regional averages, HCLIM12 underestimates Rx1d in most regions except the east and is biased towards wetter, while HCLIM3 shows relatively smaller biases in most regions except the east, due to improvements in microphysics and convection schemes (Lind et al., 2020).

Despite the overall better performance of HCLIM3, slightly larger biases in summer over the east, south and west may result from the model's sensitivity to convective processes and limitations in accurately resolving localized dynamics under moisture-rich and unstable atmospheric conditions. These challenges are particularly pronounced during summer, when the intensity of convective activity increases, leading to rapid atmospheric feedbacks and localized extremes (Poujol et al., 2021). In contrast, the southern region in winter is mainly affected by atmospheric rivers (ARs) associated to extratropical cyclones, and HCLIM3 can better capture this feature due to its finer resolution.

In terms of annual Rx1h, HCLIM3 outperforms HCLIM12, although it exhibits a wet bias compared to SeNorge2. HCLIM12 underestimates Rx1h in most grids, likely due to its reliance on parameterization schemes that fail to capture extremes (Médus et al., 2022). However, HCLIM3 shows larger biases in seasonal Rx1h in the west in all seasons except spring, and in the east and middle region in summer, the overestimation of HCLIM3 over Norway may be attributed to the underestimation in the hourly SeNorge2 (Lussana et al., 2018). Compared with daily extremes, both HCLIM3 and HCLIM12 exhibit larger biases in simulating hourly extremes compared to daily extremes, both at the annual and seasonal scales. It is important to note the limitations of the SeNorge2 dataset, which only spans eight years and is interpolated from sparse hourly rain gauges.

In summary, HCLIM3 demonstrates better agreement with observations across most regions of Norway and seasons at the regional scale, with the exception of the east and summer. This is consistent with previous studies highlighting the advantage of convection-permitting models, especially in capturing extreme precipitation events over complex terrain (Kendon et al., 2023; Médus et al., 2022; Lucas-Picher et al., 2021).

5.3 Added value of CPRCMs at local scale

The analysis of local scale convection-permitting climate models (CPRCMs) highlights their better performance in capturing precipitation extremes. HCLIM3 demonstrates notable advantages over HCLIM12, especially in terms of hourly precipitation extremes (Rx1h). For example, HCLIM3 achieves near-zero bias for the annual Rx1d in Norway (Fig. 5) and relative smaller bias for hourly extremes (Fig. 7 and Fig. 8) in all stations, while HCLIM12 consistently underestimates the return levels for hourly extremes at most station (Fig. 8) and daily extremes in all regions. Médus et al. (2022) also pointed out that RCMs underestimate the return levels of Rx1h in Norway. Thomassen et al. (2023) compared the performance of HCLIM3 and HCLIM12 based on local rain-gauge data in Denmark, and found that HCLIM12 indeed underestimate the hourly extreme event and HCLIM3 agree well with observation. Despite these benefits, the added value of HCLIM3 is not uniform across all stations and seasons, which struggle to capture summer daily extremes in the south and west, and the return level in the east and west. However, it should also be noted that the analysis is based on data from only 10 sites, which limits the generalizability of the findings to local hourly extreme events. Further studies of hourly extreme events at more stations are needed to validate these results and provide a more comprehensive understanding. Additionally, the uncertainties in the extreme precipitation analysis based on the stationary GEV method with a 20-years data series should also be noted.

The added value of CPRCMs in simulating hourly precipitation extremes is more obvious at the local scale than at the regional scale. The damped extremes caused by grid-scale averaging may explain the smaller return-level observed for HCLIM3 and HCLIM12 compared to station-level observations. As discussed in Section 5.1, this discrepancy between regional and local scales may be partly due to the inadequate density of in-situ observations.

Few studies have systematically compared hourly and daily rainfall in RCMs due to the challenges in reliably simulating hourly extremes. In line with Ban et al. (2014), we find that RCMs such as HCLIM12 demonstrate reasonably well performance for daily extremes with biases less than 50%. However, CPRCMs such as HCLIM3 perform better for hourly extremes. This is consistent with previous studies (Jiang et al., 2013; Thomassen et al., 2023), such as, Jiang et al. (2013), which showed that it is challenging to capture sub-daily extreme rainfall using RCMs with a resolution of 10 km in the southwestern United States. The better performance of CPRCMs compared to RCMs at hourly scale is consistent with the findings by Médus et al. (2022) and Ban et al. (2014), emphasizing that the CPRCMs have significantly better sub-daily precipitation characteristics, including spatial distribution and duration-intensity characteristics. Nonetheless, further improvements in the observation networks and longer observational datasets are necessary to fully verify and realize the benefits of CPRCMs at finer spatial and temporal scales.

Comparison of regional and local extreme precipitation seasonality confirms that HCLIM3 is able to represent the seasonality of daily extremes, although both HCLIM3 and HCLIM12 fail to capture the spring-summer events in the middle region. Moustakis et al. (2021) also highlighted the adequacy of CPRCMs (CTL-WRF~4 km) in capturing seasonality observed over the United States. In particular, we observe HCLIM3 better represent the seasonality of hourly precipitation at the local scale. The persistent underestimation of hourly extremes by

557   HCLIM12 may be attributed to higher uncertainty in its convective parameterization scheme or numerical
558   uncertainties at the local scale.

5.4 Added value of CPRCMs in reproducing reverse orographic effect

560   An unclear relation of daily extreme precipitation with elevation was also seen from the study of Dallan et al.
561   (2023), in which, they analyzed annual daily return level based on CPRCMs and in-situ observation over Alpine
562   region. By comparing the relationship between elevation and seasonal variation of extreme precipitation, HCLIM3
563   represents the reverse orographic effect well at regional and local scale, although there is a weak relationship
564   between extreme precipitation and elevation at the regional scale. The reverse orographic effects on hourly and daily
565   extremes vary with seasons, indicating the influence of topography on extreme precipitation at different timescales
566   and emphasizing the reliability of simulation of extreme precipitation over complex terrain. Unlike Rx1d at the
567   regional scale, which is less affected by topography, the slope of the reverse orographic effect of daily extreme
568   precipitation at the local scale is more clearly. From a seasonal perspective, the reverse orographic effect of extreme
569   precipitation in summer is not well captured in HCLIM3 and HCLIM12, which may be related to the intense
570   orographically-sustained convection affected by the atmospheric, aerosol conditions, local terrain slope and
571   shadowing effects, which RCMs and CPRCMs fail to capture (Dallan et al., 2023; Poujol et al., 2021).

572   For hourly extremes, the reverse orography effect of seasonal Rx1h in this study is consistent with the reverse
573   orographic effect of hourly return level, as found by Dallan et al. (2023) over Alpine region. HCLIM3 and
574   HCLIM12 well capture the reverse orography effect on seasonal Rx1h, especially in HCLIM3, although a stronger
575   decrease of Rx1h with elevation is observed from SeNorge2 except spring. In comparison, lower Rx1h and weak
576   reverse orography effect is found in HCLIM12 in all seasons. Our findings confirm the reverse orographic effect on
577   Rx1h, as demonstrated by Marra et al. (2021) for hourly precipitation and Formetta et al. (2022) for sub-hourly
578   scale.

579   Furthermore, we demonstrate the reverse orographic effect for both seasonal Rx1h and Rx1d, which contrasts
580   with the findings of Formetta et al. (2022), who identified a reverse orographic effect for hourly and sub-hourly
581   durations, and an orographic enhancement for durations of approximately 8 hours or longer. The "orographic
582   enhancement" (Avanzi et al., 2021; Formetta et al., 2022; Amponsah et al., 2022)—the increase in precipitation on
583   the windward side due to the lifting of air masses and the decrease on the leeward side from air descent and
584   drying—is not found in our study at either the regional or local scales. These results deviate from the anticipated
585   patterns, which may be attributed to the combined effects of latitude, climate, altitude zones, static atmospheric or
586   aerosol conditions, and shadowing effects (Amponsah et al., 2022; Napoli et al., 2019).

587   It should be noted that simple relationship between extreme precipitation and elevation is difficult to build due
588   to several land surface characteristics could influence the precipitation, a complex regression model should be
589   considered to more realistically quantify the reverse orographic effect (Zhang et al., 2018) in the future. The
590   interpolated gridded dataset and limited rain gauges over the complex orography, along with the decreasing station
591   density at higher elevations, may also limit the reliable analysis of the reverse orographic effect. The sparsity of rain

592   gauges and under catch problems could also lead to underestimation of precipitation, especially in the complex

593   orography (Lussana et al., 2018, 2019; Gervais et al., 2014b).

594   **6 Conclusions**

595   In this study, we conducted a comprehensive evaluation of extreme precipitation characteristics from regional to

596   local scale in Norway, focusing on five distinct regions, utilizing a convection-permitting regional climate model

597   (HCLIM3) and comparing it with its convection-parameterized regional climate model (HCLIM12) forced by ERA-

598   Interim data during 1999-2018.

599   The key conclusions of this study are as follows:

600   a) At regional scale, HCLIM3 shows consistent advantage in capturing Rx1d, compared to HCLIM12, with

601   improved representation of Rx1d in most regions and season, while HCLIM12 underestimates the annual

602   daily extremes in all regions except the east. Specifically, HCLIM3 shows larger bias of Rx1d in summer

603   over east, south and west regions, and the return level of daily extreme in the eastern region. In

604   comparison, for hourly extremes, HCLIM3 captures Rx1h better in most regions and seasons except the

605   west and the summer compared to HCLIM12. In general, HCLIM3 overestimates the annual Rx1h while

606   HCLIM12 underestimates it. Besides, HCLIM3 and HCLIM12 show larger bias in percentage for hourly

607   extremes than daily extremes.

608   b) At local scale, HCLIM3 shows added value in capturing the annual and seasonal Rx1d in most regions,

609   compared to HCLIM12. Specifically, HCLIM3 can better capture the return levels of daily extremes in

610   most regions except in the west and east, and it shows smaller biases in Rx1d across Norway for all

611   seasons, except summer in the southern and western regions. Overall, HCLIM3 shows consistent benefit

612   in capturing the daily extremes in the middle and north regions compared with HCLIM12, both at the

613   regional and local scales. For hourly extreme precipitation, HCLIM3 outperforms HCLIM12 in capturing

614   the annual Rx1h and return levels in those 10 stations.

615   c) For the seasonality of extremes, at the regional scale, HCLIM3 and HCLIM12 can well characterize the

616   seasonality of daily extremes except for the middle region, especially for HCLIM3 in the western region.

617   At local scale, the seasonality of Rx1d can also be captured by HCLIM3 and HCLIM12. A distinct

618   advantage emerges with HCLIM3 for hourly extremes, where it accurately reflects both the occurrence

619   and intensity of these events across different seasons, while HCLIM12 tends to underestimate these

620   aspects.

621   d) In Norway, the effect of the preserved topography on seasonal Rx1h and Rx1d emerge from regional to

622   local scales, although weak relationship between Rx1d and elevation is demonstrated at regional scale. For

623   seasonal Rx1h, both HCLIM3 and HCLIM12 can capture the reverse orographic effect at regional scale,

624   but no added value is shown in HCLIM3. In particular, at the local scale, the reverse orographic effect of

625   seasonal Rx1d is more pronounced, and HCLIM3 provides added value in all seasons except summer.

Acknowledgments

We would like to thank Stefan P. Sobolowski, for his great support as PI of the EU Impetus4change (I4C) project. This research was supported by the European Union's Horizon 2020 research, innovation programme under grant agreement no. 101081555 (IMPETUS4CHANGE) and the Research Council of Norway through FRINATEK Project 274310. The computer resources where available through the RCN's program for supercomputing (NOTUR/NORSTORE); projects NN10014K and NS10014K. All simulation data in this paper are available from the authors upon request (luli@norceresearch.no).

Competing interests. The authors declare that they have no conflict of interest.

References

Adinolfi, M., Raffa, M., Reder, A., and Mercogliano, P.: Evaluation and Expected Changes of Summer Precipitation at Convection Permitting Scale with COSMO-CLM over Alpine Space, 10.3390/atmos12010054, 2021.

Amponsah, W., Dallan, E., Nikolopoulos, E. I., and Marra, F.: Climatic and altitudinal controls on rainfall extremes and their temporal changes in data-sparse tropical regions. Journal of Hydrology 612, 128090. https://doi.org/10.1016/j.jhydrol.2022.128090, 2022.

Avanzi, F., Ercolani, G., Gabellani, S., Cremonese, E., Pogliotti, P., Filippa, G., Morra di Cella, U., Ratto, S., Stevenin, H., Cauduro, M., and Juglair, S.: Learning about precipitation lapse rates from snow course data improves water balance modeling, Hydrol. Earth Syst. Sci., 25, 2109-2131, 10.5194/hess-25-2109-2021, 2021.

Ban, N., Schmidli, J., and Schär, C.: Evaluation of the convection-resolving regional climate modeling approach in decade-long simulations, Journal of Geophysical Research: Atmospheres, 119, 7889-7907, https://doi.org/10.1002/2014JD021478, 2014.

Ban, N., Rajczak, J., Schmidli, J., and Schär, C.: Analysis of Alpine precipitation extremes using generalized extreme value theory in convection-resolving climate simulations, Climate Dynamics, 55, 61-75, 10.1007/s00382-018-4339-4, 2020.

Chapman, S., Bacon, J., Birch, C. E., Pope, E., Marsham, J. H., Msemo, H., Nkonde, E., Sinachikupo, K., and Vanya, C.: Climate Change Impacts on Extreme Rainfall in Eastern Africa in a Convection-Permitting Climate Model, Journal of Climate, 36, 93-109, https://doi.org/10.1175/JCLI-D-21-0851.1, 2023.

Coles, S., Pericchi, L. R., and Sisson, S.: A fully probabilistic approach to extreme rainfall modeling, Journal of Hydrology, 273, 35-50, https://doi.org/10.1016/S0022-1694(02)00353-0, 2003.

Dallan, E., Marra, F., Fosser, G., Marani, M., Formetta, G., Schär, C., and Borga, M.: How well does a convection-permitting regional climate model represent the reverse orographic effect of extreme hourly precipitation?, Hydrol. Earth Syst. Sci., 27, 1133-1149, 10.5194/hess-27-1133-2023, 2023.

Di Piazza, A., Conti, F. L., Noto, L. V., Viola, F., and La Loggia, G.: Comparative analysis of different techniques for spatial interpolation of rainfall data to create a serially complete monthly time series of precipitation for

Sicily, Italy, International Journal of Applied Earth Observation and Geoinformation, 13, 396-408, https://doi.org/10.1016/j.jag.2011.01.005, 2011.

Dyrrdal, A. V., Médus, E., Dobler, A., Hodnebrog, Ø., Arnbjerg-Nielsen, K., Olsson, J., Thomassen, E. D., Lind, P., Gaile, D., and Post, P.: Changes in design precipitation over the Nordic-Baltic region as given by convection-permitting climate simulations, Weather and Climate Extremes, 42, 100604, 10.1016/j.wace.2023.100604, 2023.

Formetta, G., Marra, F., Dallan, E., Zaramella, M., and Borga, M.: Differential orographic impact on sub-hourly, hourly, and daily extreme precipitation. Advances in Water Resources 159, 104085. https://doi.org/10.1016/j.advwatres.2021.104085, 2022.

Gervais, M., Gyakum, J. R., Atallah, E., Tremblay, L. B., and Neale, R. B.: How Well Are the Distribution and Extreme Values of Daily Precipitation over North America Represented in the Community Climate System Model? A Comparison to Reanalysis, Satellite, and Gridded Station Data, Journal of Climate, 27, 5219-5239, https://doi.org/10.1175/JCLI-D-13-00320.1, 2014a.

Gervais, M., Tremblay, L. B., Gyakum, J. R., and Atallah, E.: Representing Extremes in a Daily Gridded Precipitation Analysis over the United States: Impacts of Station Density, Resolution, and Gridding Methods, Journal of Climate, 27, 5201-5218, https://doi.org/10.1175/JCLI-D-13-00319.1, 2014b.

Giordani, A., Cerenzia, I. M. L., Paccagnella, T., and Di Sabatino, S.: SPHERA, a new convection-permitting regional reanalysis over Italy: Improving the description of heavy rainfall, Quarterly Journal of the Royal Meteorological Society, 149, 781-808, https://doi.org/10.1002/qj.4428, 2023.

Jiang, P., Gautam, M. R., Zhu, J., and Yu, Z.: How well do the GCMs/RCMs capture the multi-scale temporal variability of precipitation in the Southwestern United States?, Journal of Hydrology, 479, 75-85, https://doi.org/10.1016/j.jhydrol.2012.11.041, 2013.

Kendon, E. J., Fischer, E. M., and Short, C. J.: Variability conceals emerging trend in 100yr projections of UK local hourly rainfall extremes, Nature Communications, 14, 1133, 10.1038/s41467-023-36499-9, 2023.

Kendon, E. J., Stratton, R. A., Tucker, S., Marsham, J. H., Berthou, S., Rowell, D. P., and Senior, C. A.: Enhanced future changes in wet and dry extremes over Africa at convection-permitting scale, Nature Communications, 10, 1794, 10.1038/s41467-019-09776-9, 2019.

Kent, C., Dunstone, N., Tucker, S., Scaife, A. A., Brown, S., Kendon, E. J., Smith, D., McLean, L., and Greenwood, S.: Estimating unprecedented extremes in UK summer daily rainfall, Environmental Research Letters, 17, 014041, 10.1088/1748-9326/ac42fb, 2022.

Kim, Y., Rocheta, E., Evans, J. P., and Sharma, A.: Impact of bias correction of regional climate model boundary conditions on the simulation of precipitation extremes, Climate Dynamics, 55, 3507-3526, 10.1007/s00382-020-05462-5, 2020.

Knist, S., Goergen, K., and Simmer, C.: Evaluation and projected changes of precipitation statistics in convection-permitting WRF climate simulations over Central Europe, Climate Dynamics, 55, 325-341, 10.1007/s00382-018-4147-x, 2020.

697 Konstali, K. and Sorteberg, A.: Why has Precipitation Increased in the Last 120 Years in Norway?, Journal of
698   Geophysical Research: Atmospheres, 127, 10.1029/2021jd036234, 2022.

699 Li, J., Gan, T. Y., Chen, Y. D., Gu, X., Hu, Z., Zhou, Q., and Lai, Y.: Tackling resolution mismatch of precipitation
700   extremes from gridded GCMs and site-scale observations: Implication to assessment and future projection,
701   Atmospheric Research, 239, 104908, https://doi.org/10.1016/j.atmosres.2020.104908, 2020a.

702 Li, L., Pontoppidan, M., Sobolowski, S., and Senatore, A.: The impact of initial conditions on convection-permitting
703   simulations of a flood event over complex mountainous terrain, Hydrol. Earth Syst. Sci., 24, 771-791,
704   10.5194/hess-24-771-2020, 2020b.

705 Li, P., Furtado, K., Zhou, T., Chen, H., and Li, J.: Convection-permitting modelling improves simulated
706   precipitation over the central and eastern Tibetan Plateau, Quarterly Journal of the Royal Meteorological
707   Society, 147, 341-362, https://doi.org/10.1002/qj.3921, 2021.

708 Lind, P., Lindstedt, D., Kjellström, E., and Jones, C.: Spatial and Temporal Characteristics of Summer Precipitation
709   over Central Europe in a Suite of High-Resolution Climate Models, Journal of Climate, 29, 3501-3518,
710   https://doi.org/10.1175/JCLI-D-15-0463.1, 2016.

711 Lind, P., Belušić, D., Christensen, O. B., Dobler, A., Kjellström, E., Landgren, O., Lindstedt, D., Matte, D.,
712   Pedersen, R. A., Toivonen, E., and Wang, F.: Benefits and added value of convection-permitting climate
713   modeling over Fenno-Scandinavia, Climate Dynamics, 55, 1893-1912, 10.1007/s00382-020-05359-3,
714   2020.

715 Liu, C., Ikeda, K., Rasmussen, R., Barlage, M., Newman, A. J., Prein, A. F., Chen, F., Chen, L., Clark, M., Dai, A.,
716   Dudhia, J., Eidhammer, T., Gochis, D., Gutmann, E., Kurkute, S., Li, Y., Thompson, G., and Yates, D.:
717   Continental-scale convection-permitting modeling of the current and future climate of North America,
718   Climate Dynamics, 49, 71-95, 10.1007/s00382-016-3327-9, 2017.

719 Lucas-Picher, P., Argüeso, D., Brisson, E., Tramblay, Y., Berg, P., Lemonsu, A., Kotlarski, S., and Caillaud, C.:
720   Convection-permitting modeling with regional climate models: Latest developments and next steps. WIREs
721   Climate Change 12(6), e731. https://doi.org/10.1002/wcc.731, 2021.

722 Lussana, C., Tveito, O. E., Dobler, A., and Tunheim, K.: seNorge_2018, daily precipitation, and temperature
723   datasets over Norway, Earth Syst. Sci. Data, 11, 1531-1551, 10.5194/essd-11-1531-2019, 2019.

724 Lussana, C., Saloranta, T., Skaugen, T., Magnusson, J., Tveito, O. E., and Andersen, J.: seNorge2 daily
725   precipitation, an observational gridded dataset over Norway from 1957 to the present day, Earth Syst. Sci.
726   Data, 10, 235-249, 10.5194/essd-10-235-2018, 2018.

727 Mahoney, K., Ralph, F. M., Wolter, K., Doesken, N., Dettinger, M., Gottas, D., Coleman, T., and White, A.:
728   Climatology of Extreme Daily Precipitation in Colorado and Its Diverse Spatial and Seasonal Variability,
729   Journal of Hydrometeorology, 16, 781-792, https://doi.org/10.1175/JHM-D-14-0112.1, 2015.

730 Marra, F., Armon, M., Borga, M., and Morin, E.: Orographic Effect on Extreme Precipitation Statistics Peaks at
731   Hourly Time Scales, Geophysical Research Letters, 48, e2020GL091498,
732   https://doi.org/10.1029/2020GL091498, 2021.

733 Médus, E., Thomassen, E. D., Belušić, D., Lind, P., Berg, P., Christensen, J. H., Christensen, O. B., Dobler, A.,
734   Kjellström, E., Olsson, J., and Yang, W.: Characteristics of precipitation extremes over the Nordic region:
735   added value of convection-permitting modeling, Nat. Hazards Earth Syst. Sci., 22, 693-711, 10.5194/nhess-
736   22-693-2022, 2022.
737 Michel, C., Sorteberg, A., Eckhardt, S., Weijenborg, C., Stohl, A., and Cassiani, M.: Characterization of the
738   atmospheric environment during extreme precipitation events associated with atmospheric rivers in Norway
739   - Seasonal and regional aspects, Weather and Climate Extremes, 34, 100370, 10.1016/j.wace.2021.100370,
740   2021.
741 Moustakis, Y., Papalexiou, S. M., Onof, C. J., and Paschalis, A.: Seasonality, Intensity, and Duration of Rainfall
742   Extremes Change in a Warmer Climate, Earth's Future, 9, e2020EF001824,
743   https://doi.org/10.1029/2020EF001824, 2021.
744 Napoli, A., Crespi, A., Ragone, F., Maugeri, M., and Pasquero, C.: Variability of orographic enhancement of
745   precipitation in the Alpine region. Scientific Reports 9(1), 13352. 10.1038/s41598-019-49974-5, 2019.
746 Piani, C., Weedon, G. P., Best, M., Gomes, S. M., Viterbo, P., Hagemann, S., and Haerter, J. O.: Statistical bias
747   correction of global simulated daily precipitation and temperature for the application of hydrological
748   models, Journal of Hydrology, 395, 199-215, https://doi.org/10.1016/j.jhydrol.2010.10.024, 2010.
749 Pontoppidan, M., Kolstad, E. W., Sobolowski, S., and King, M. P.: Improving the Reliability and Added Value of
750   Dynamical Downscaling via Correction of Large-Scale Errors: A Norwegian Perspective, Journal of
751   Geophysical Research: Atmospheres, 123, 11,875-811,888, 10.1029/2018jd028372, 2018.
752 Poujol, B., Mooney, P. A., and Sobolowski, S. P.: Physical processes driving intensification of future precipitation
753   in the mid- to high latitudes, Environmental Research Letters, 16, 034051, 10.1088/1748-9326/abdd5b,
754   2021.
755 Prein, A. F., Langhans, W., Fosser, G., Ferrone, A., Ban, N., Goergen, K., Keller, M., Tölle, M., Gutjahr, O., Feser,
756   F., Brisson, E., Kollet, S., Schmidli, J., van Lipzig, N. P. M., and Leung, R.: A review on regional
757   convection-permitting climate modeling: Demonstrations, prospects, and challenges, Reviews of
758   Geophysics, 53, 323-361, https://doi.org/10.1002/2014RG000475, 2015.
759 Reder, A., Raffa, M., Montesarchio, M., and Mercogliano, P.: Performance evaluation of regional climate model
760   simulations at different spatial and temporal scales over the complex orography area of the Alpine region,
761   Natural Hazards, 102, 151-177, 10.1007/s11069-020-03916-x, 2020.
762 Rossi, M. W., Anderson, R. S., Anderson, S. P., and Tucker, G. E.: Orographic Controls on Subdaily Rainfall
763   Statistics and Flood Frequency in the Colorado Front Range, USA, Geophysical Research Letters, 47,
764   e2019GL085086, https://doi.org/10.1029/2019GL085086, 2020.
765 Tabari, H.: Climate change impact on flood and extreme precipitation increases with water availability, Scientific
766   Reports, 10, 13768, 10.1038/s41598-020-70816-2, 2020.
767 Thackeray, C. W., Hall, A., Norris, J., and Chen, D.: Constraining the increased frequency of global precipitation
768   extremes under warming, Nature Climate Change, 12, 441-448, 10.1038/s41558-022-01329-1, 2022.

769   Thomassen, E. D., Arnbjerg-Nielsen, K., Sørup, H. J. D., Langen, P. L., Olsson, J., Pedersen, R. A., and

770   Christensen, O. B.: Spatial and temporal characteristics of extreme rainfall: Added benefits with sub-

771   kilometre-resolution climate model simulations?, Quarterly Journal of the Royal Meteorological Society,

772   149, 1913-1931, https://doi.org/10.1002/qj.4488, 2023.

773   Wang, Y., Zhang, G. J., and He, Y.-J.: Simulation of Precipitation Extremes Using a Stochastic Convective

774   Parameterization in the NCAR CAM5 Under Different Resolutions, Journal of Geophysical Research:

775   Atmospheres, 122, 12,875-812,891, https://doi.org/10.1002/2017JD026901, 2017.

776   Zhang, T., Li, B., Yuan, Y., Gao, X., Sun, Q., Xu, L., and Jiang, Y.: Spatial downscaling of TRMM precipitation

777   data considering the impacts of macro-geographical factors and local elevation in the Three-River

778   Headwaters Region, Remote Sensing of Environment, 215, 109-127,

779   https://doi.org/10.1016/j.rse.2018.06.004, 2018.

780   Vormoor, K., Lawrence, D., Schlichting, L., Wilson, D., and Wong, W. K.: Evidence for changes in the magnitude

781   and frequency of observed rainfall vs. snowmelt driven floods in Norway, Journal of Hydrology, 538, 33-

782   48, 10.1016/j.jhydrol.2016.03.066, 2016.

783   Whan, K., Sillmann, J., Schaller, N., and Haarsma, R.: Future changes in atmospheric rivers and extreme

784   precipitation in Norway. Climate Dynamics 54(3), 2071-2084. 10.1007/s00382-019-05099-z, 2020.

785

786 **Supplement**

Enhanced Evaluation of hourly and Daily Extreme Precipitation in Norway from Convection-Permitting Models at Regional and Local Scales

791 Kun Xie[1,2], Lu Li[3], Hua Chen[1,2], Stephanie Mayer[3], Andreas Dobler[4], Chong-Yu Xu[5], Ozan Mert Gokturk[3]

793 [1]State Key Laboratory of Water Resources and Hydropower Engineering Science, Wuhan University, Wuhan

794 430072, P. R. China

795 [2]Hubei Provincial Key Lab of Water System Science for Sponge City Construction, Wuhan University, Wuhan,

796 China

797 [3]NORCE Norwegian Research Centre, Bjerknes Centre for Climate Research, Bergen, Norway

798 [4]The Norwegian Meteorological Institute, Oslo, Norway

799 [5]Department of Geosciences, University of Oslo, P.O Box 1047 Blindern, 0316 Oslo, Norway

801 *Correspondence to*: Hua Chen (chua@whu.edu.cn); Lu Li (luli@norceresearch.no)

803

804 **Table S1. The information for the ten hourly rain gauges.**

Name	Station ID	Longitude (°E)	Latitude (°N)	Elevation(m)	Region
Østre Toten - Apelsvoll	SN11500	10.8695	60.7002	264	East
Ås - Rustadskogen	SN17870	10.8107	59.6703	120	East
Kise in Hedmark	SN12550	10.8055	60.7733	128	East
Løken i Volbu	SN23500	9.063	61.122	521	East
Kvithamar	SN69150	10.8795	63.4882	27	Middle
Tjøtta	SN76530	12.4255	65.8295	21	Middle
Stryn - Kroken	SN58900	6.5585	61.9157	208	West
Fureneset	SN56420	5.0443	61.2928	7	West
Særheim	SN44300	5.6508	58.7605	87	South
Tromsø - Holt	SN90400	18.9095	69.6538	20	North

805
806

807 **Table S2. The information for the 192 daily rain gauges.**

ID	Name	Longitude (°E)	Latitude (°N)	Elevation (m)	ID	Name	Longitude (°E)	Latitude (°N)	Elevation (m)
SN420	HEGGERISET -	11.9963	61.6848	481	SN98550	VARDØ RADIO	31.0962	70.3707	10
SN78370	BJERKA - VALLA	13.8067	66.1415	20	SN47090	SKJOLD - FRØVIK	5.6257	59.5033	5
SN47820	EIKEMO	6.2786	59.8594	178	SN69960	BURAN	11.5436	63.7199	182
SN82290	BODØ VI	14.3816	67.2723	16	SN44480	SØYLAND I GJESDAL	5.9817	58.6855	263
SN32780	HØIDALEN I SOLUM	9.2668	59.1444	113	SN810	TUFSINGDAL - MIDTDAL	11.732	62.2776	687
SN63580	ÅNGÅRDSVATNET	9.1967	62.6708	596	SN50150	HATLESTRAND	5.9032	60.045	45
SN43810	MAUDAL	6.3675	58.7645	311	SN78350	BARDAL	13.3917	66.2178	39
SN42520	RISNES I FJOTLAND	6.9443	58.6577	348	SN52860	TAKLE	5.3813	61.0272	38
SN67150	LEINSTRAND	10.2733	63.3281	13	SN24960	GOL - STAKE	8.9478	60.7188	542
SN78250	LEIRFJORD	12.9097	66.0668	53	SN34900	POSTMYR I DRANGEDAL	8.7687	59.2647	464
SN42810	TONSTAD - NETTFED	6.709	58.6642	55	SN76100	ØKSNINGØY	12.3745	65.1245	24
SN36490	BØYLEFOSS	8.717	58.5967	63	SN82530	KJERRINGØY - OS	14.8402	67.5385	15
SN68270	LØKSMYR	10.4369	63.2315	173	SN25100	HEMSEDAL - HØLTO	8.5285	60.8703	648
SN46150	SAND I RYFYLKE II	6.276	59.4791	25	SN730	VALDALEN	12.1722	62.0758	794
SN8720	ATNSJØEN	10.1398	61.8902	749	SN72650	OVERHALLA - UNNSET	11.8397	64.4815	26
SN70820	UTGÅRD	11.729	64.1163	50	SN61040	HILDRE	6.3187	62.6017	13
SN47450	STRAUMØY	5.4335	59.6532	36	SN52930	BREKKE I SOGN	5.425	60.9585	240
SN31080	TESSUNGDALEN -	8.7033	60.1293	762	SN52170	EKSINGEDAL	6.1469	60.8028	450
SN48500	ROSENDAL	6.02637	59.9913	75	SN31410	RJUKAN	8.6663	59.88	258
SN33250	RAULAND	8.0317	59.7057	719	SN60500	TAFJORD	7.4218	62.2305	11
SN66620	RENNEBU - RAMSTAD	9.8354	62.864	223	SN93900	SIHCCAJAVRI	23.5387	68.7553	382
SN82840	STYRKESNES - HESTVIKA	15.4953	67.5258	27	SN60400	NORDDAL	7.2392	62.2477	28
SN770	ELLEFSPLASS	11.4525	62.204	713	SN32850	KVITESEID - MOEN	8.473	59.4058	76
SN57810	SVELGEN II	5.2983	61.7707	16	SN38380	DOVLAND	8.0392	58.5234	259
SN96970	SIRBMA	27.4018	70.0185	51	SN92350	NORDSTRAUM I	21.8958	69.8362	20
SN76250	SØMNA - STEIN	12.1643	65.2965	19	SN14050	SJOA	9.5562	61.6757	330
SN13420	VENABU	10.1082	61.6513	930	SN73500	NORDLI - HOLAND	13.718	64.4458	433
SN40420	BYKLE - KULTRAN	7.3438	59.3505	594	SN43010	EIK - HOVE	6.5045	58.507	65
SN88660	BOTNHAMN	17.9175	69.5212	6	SN41550	LJOSLAND - MONEN	7.3501	58.7878	504
SN12600	VEA	10.6791	60.953	161	SN41770	LINDESNES FYR	7.048	57.9815	16
SN38800	TOVDAL	8.2295	58.7938	220	SN83300	STEIGEN	15.1123	67.923	31
SN71550	ØRLAND III	9.6105	63.7045	10	SN18700	OSLO - BLINDERN	10.72	59.9423	94
SN75020	OTTERØY	11.2806	64.5228	36	SN59900	SÆBØ	6.4657	62.2027	21
SN44760	IMS	5.9672	58.9055	2	SN55670	VEITASTROND	7.034	61.4783	172
SN77850	SUSENDAL	14.2457	65.3675	498	SN63530	HAFSÅS	8.9773	62.5095	698
SN31570	MØSVATN - HAUG	8.1342	59.8143	945	SN73250	SØRLI	13.765	64.2432	370
SN100	PLASSEN	12.5039	61.1349	333	SN3780	IGSI I HOBØL	11.0468	59.636	144
SN37230	TVEITSUND	8.5187	59.0257	252	SN88100	BONES I BARDU	18.2442	68.6457	230
SN92910	SOPNESBUKT	22.3243	70.0518	8	SN52990	ORTNEVIK	6.134	61.1095	4
SN60990	VIGRA	6.115	62.5617	22	SN58480	OLDEDALEN	6.8088	61.694	44
SN44560	SOLA	5.637	58.8843	7	SN63750	MJØEN	9.6591	62.574	512
SN80610	MYKEN	12.486	66.7628	17	SN20520	LUNNER	10.5753	60.295	372
SN22730	HEDAL I VALDRES II	9.7238	60.6197	474	SN36560	NELAUG	8.63	58.6582	142
SN79480	MO I RANA III	14.1542	66.307	41	SN53130	FRESVIK	6.9345	61.0688	32
SN39220	MESTAD I ODDERNES	7.89	58.2153	151	SN48450	HUSNES	5.7694553	59.8641203	13
SN89350	BARDUFOSS	18.5437	69.0577	76	SN10600	AURSUND	11.4534	62.6737	685
SN1230	HALDEN	11.388	59.1223	3	SN24600	GRIMELI I KRØDSHERAD	9.5958	60.137	367
SN53160	JORDALEN - NÅSEN	6.7243	60.9004	614	SN4780	GARDERMOEN	11.0802	60.2065	202

808
809

   Table S2. Continue.

ID	Name	Longitude (°E)	Latitude (°N)	Elevation (m)	ID	Name	Longitude (°E)	Latitude (°N)	Elevation (m)
SN16610	FOKSTUGU	9.2862	62.1133	973	SN93700	KAUTOKEINO	23.0335	68.9968	307
SN58320	MYKLEBUST I BREIM	6.6092	61.708	315	SN59250	REFVIK	5.0878	61.9985	3
SN69100	VÆRNES	10.9305	63.4597	12	SN46300	SULDALSVATN	6.809	59.5887	333
SN80740	REIPÅ	13.646	66.9035	9	SN22840	REINLI	9.4905	60.8346	628
SN57940	ÅLFOTEN II	5.6674	61.832	24	SN51250	ØVSTEDAL	5.9647	60.6887	316
SN60620	GRØNNING	7.5135	62.3292	312	SN52750	FRØYSET	5.2108	60.8462	13
SN58780	NORDFJORDEID - NYMARK	6.0392	61.9183	34	SN12550	KISE PA HEDMARK	10.8055	60.7733	128
SN73800	TUNNSJØ	13.6506	64.6837	376	SN54600	MARISTOVA	8.0368593	61.1098838	806
SN56780	SYGNA	5.7265	61.3435	45	SN71810	ÅFJORD - MOMYR	10.523	64.1003	280
SN65230	HEMNE - LENES	9.0115	63.2613	45	SN84190	SKJOMEN - STIBERG	17.5145	68.2075	29
SN56520	HOVLANDSDAL	5.4342	61.232	85	SN57850	DAVIKNES	5.5333	61.8986	78
SN5350	NORD-ODAL	11.558	60.3883	147	SN38600	MYKLAND	8.2888	58.633	245
SN90490	TROMSØ - LANGNES	18.9133	69.6767	8	SN71200	MOSVIK -	10.998	63.8128	39
SN56850	VIKSDALEN I GAULAR	6.1983	61.3262	243	SN11710	EINAVATN	10.6408	60.59505	406
SN75100	LIAFOSS	11.9547	64.8382	44	SN57480	BOTNEN I FØRDE	6.0586	61.5349	237
SN1950	ØRJE	11.6506	59.4829	123	SN37500	FOLDSÆ	8.1517	59.3242	492
SN50540	BERGEN - FLORIDA	5.3327	60.383	12	SN52400	EIKANGER - MYR	5.3742	60.6268	72
SN31660	MOGEN	7.913	60.018	954	SN13140	FÅVANG - TROMSNES	10.1902	61.4567	187
SN9870	BLANKTJERNMOEN I	10.428	62.4343	692	SN61820	ERESFJORD	8.105	62.663	14
SN53700	AURLAND	7.201	60.9027	15	SN14550	PRESTSTULEN	9.0084	61.9225	823
SN80200	LURØY	13.1848	66.3892	115	SN86500	SORTLAND	15.4157	68.7033	3
SN71900	BESSAKER	10.3257	64.2448	12	SN11900	BIRI	10.5954	60.9518	190
SN68420	AUNET	11.5669	63.0556	302	SN41860	KVINESHEI -	6.9821926	58.2431584	317
SN27600	SANDEFJORD	10.2147	59.132	6	SN23720	VANG I VALDRES	8.569	61.124	489
SN25320	ÅL III	8.5609	60.6391	720	SN57390	SKEI I JØLSTER	6.4873	61.5722	205
SN58960	HORNINDAL	6.6502	62.0033	349	SN63100	ØKSENDAL	8.4218	62.6855	47
SN56400	YTRE SOLUND	4.6693	61.007	3	SN57990	GJENGEDAL	5.9468	61.6594	230
SN15480	SKJÅK II	8.4672	61.8777	374	SN97350	CUOVDDATMOHKKI	24.4312	69.3695	286
SN4040	ENEBAKK - BARBØL	11.1535	59.75	164	SN23560	BEITO	8.8557	61.2433	754
SN15430	BØVERDAL	8.2423	61.7195	700	SN55550	HAFSLO	7.1887	61.2925	246
SN70930	SNÅSA - NAGELHUS	12.4393	64.249	107	SN46450	RØLDAL	6.8238	59.8305	388
SN29600	TUNHOVD	8.7511	60.4629	870	SN57660	EIMHJELLEN	5.8157	61.6407	176
SN15660	SKJÅK	8.1706	61.9013	432	SN62900	EIDE PÅ NORDMØRE	7.3896	62.8909	49
SN4740	UKKESTAD	11.051	60.1742	187	SN27800	HEDRUM	9.9641	59.196	31
SN34800	TØRDAL - SUVDØLA	8.7742	59.1482	235	SN90450	TROMSØ	18.9368	69.6537	100
SN16790	LESJA - SVANBORG	8.919	62.1057	551	SN1650	STRØMSFOSS SLUSE	11.6599	59.3006	113
SN42720	BAKKE	6.657	58.4117	75	SN42650	FLEKKEFJORD	6.6498	58.28415	5
SN55730	SOGNDAL - SELSENG	6.9335	61.3348	421	SN24210	SOKNA II	9.9267	60.238	140
SN7660	ÅKRESTRØMMEN	11.2042	61.696	260	SN15730	BRÅTÅ - SLETTOM	7.8955	61.8957	664
SN71280	LEKSVIK - MYRAN	10.6075	63.6856	138	SN53070	VIK I SOGN III	6.5813	61.0728	65
SN68840	STUGUDAL - KÅSEN	11.8626	62.8952	730	SN18160	NORDSTRAND	10.7912	59.873	118
SN6440	VERMUNDSJØEN	12.369	60.6925	276	SN27770	STOKKE - SOLLI	10.2022	59.2752	90
SN60	LINNES	12.499	61.5581	564	SN90650	GRUNNFJORD -	19.573	70.0083	7
SN44800	SVILAND	5.9202	58.8185	230	SN47890	OPSTVEIT	6.0169242	59.8577805	38
SN83520	TØMMERNESET	15.859	67.8918	70	SN62700	HUSTADVATN	7.2436	62.9087	80
SN35090	EIKELAND	9.098	58.8037	42	SN41480	ÅSERAL	7.4128	58.6172	268
SN44520	HELLAND I GJESDAL	6.0135	58.755	288	SN36200	TORUNGEN FYR	8.7893	58.3988	12
SN19710	ASKER	10.4358	59.8558	163	SN56320	LAVIK	5.5413	61.1124	26

811

812
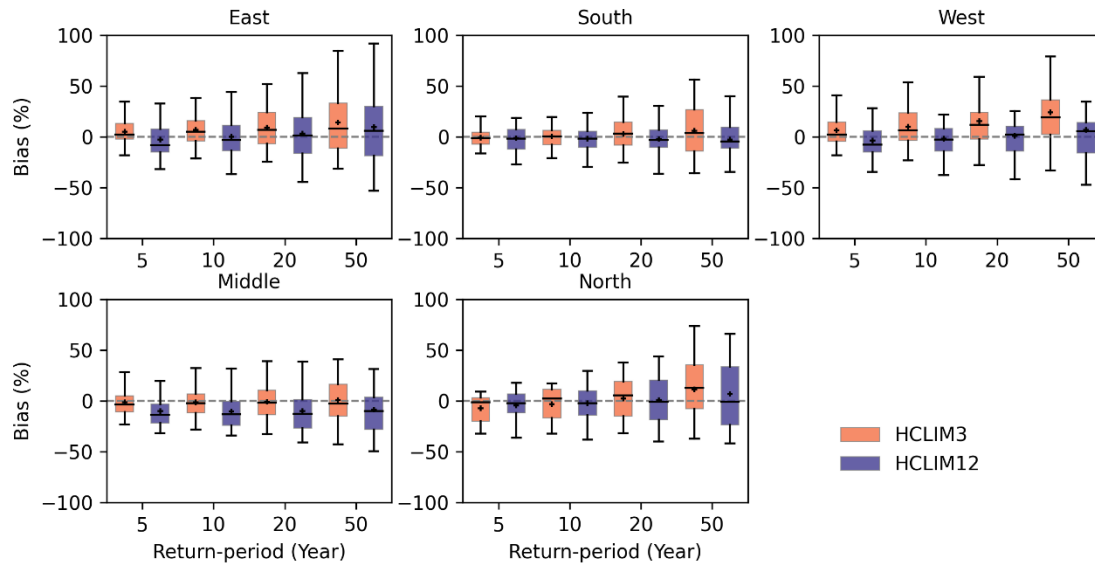
813
814 **Figure S1: Bias of return-levels in the present-day for HCLIM3 and HCLIM12 relative to observation for 5-, 10-, 20-, and**
815 **50-year return periods in the 192 daily rain-gauges. Return periods of 5-, 10-, 20-, and 50-year are calculated on the basis**
816 **of station-scale GEV. The bias of return-levels for 192-rain-gauges are statistics by regions.**
817
818
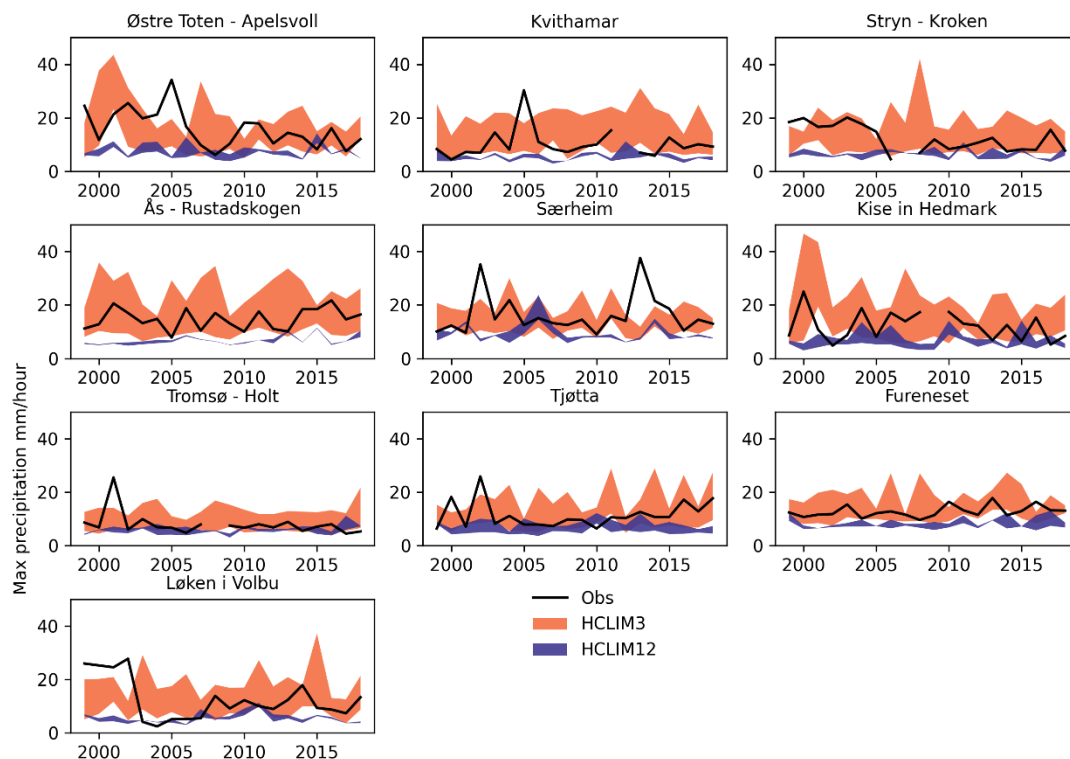
819
820 **Figure S2: Time evolution of annual maximum hourly precipitation from observation, HCLIM3 and HCLIM12 during**
821 **1999-2018 at 10 hourly rain-gauges. Grids within a 12 km radius of each station are extracted for HCLIM3 and**
822 **HCLIM12 to calculate the range band.**
823

824
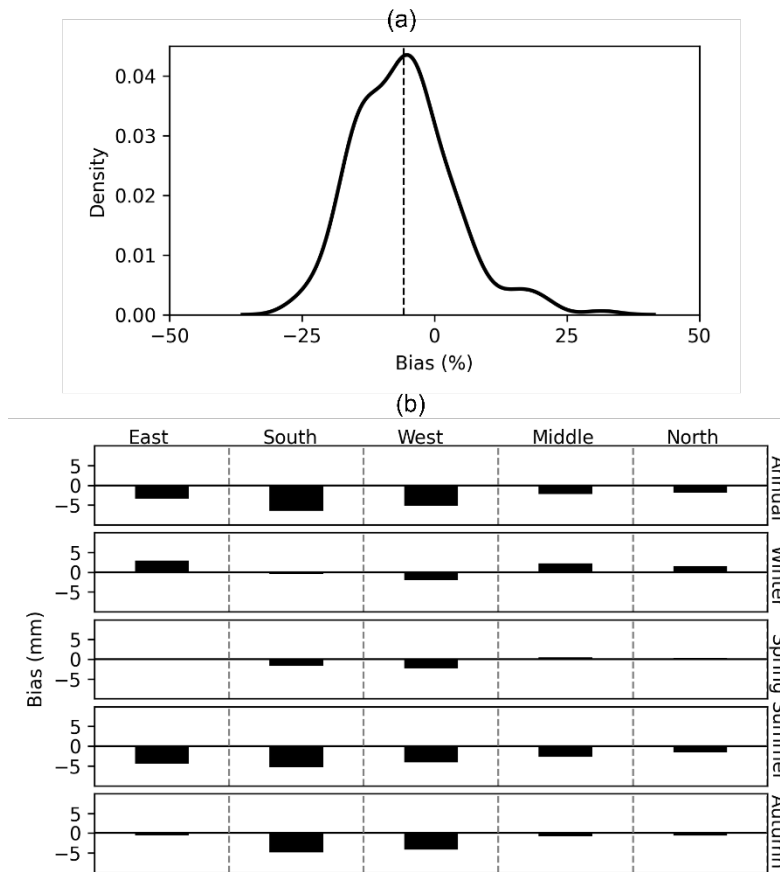
825 **Figure S3: (a) Density distribution of bias for Rx1d between SeNorge and daily in-situ observations from 194 stations**
826 **during 1999-2018; (b) the percentage difference of seasonal Rx1d between SeNorge and daily in-situ observations across**
827 **the five regions. The bias is calculated as the SeNorge minus daily in-situ observations at each station and then the**
828 **regional averages are computed.**